UNLV Retrospective Theses & Dissertations

1-1-2006

Evidence of an active Enso and Pdo during the mid-Holocene from a Costa Rican speleothem

April Dianne Azouz
University of Nevada, Las Vegas

Follow this and additional works at: https://digitalscholarship.unlv.edu/rtds

EVIDENCE OF AN ACTIVE ENSO AND PDO DURING THE MID-

HOLOCENE FROM A COSTA RICAN SPELEOTHEM

by

April Dianne Azouz

Bachelor of Science
Boston University
2004

A thesis submitted in partial fulfillment
of the requirements for the

Master of Science Degree in Geoscience
Department of Geoscience
College of Sciences

Graduate College
University of Nevada, Las Vegas
August 2006

UMI Number: 1439967

INFORMATION TO USERS

The quality of this reproduction is dependent upon the quality of the copy
submitted. Broken or indistinct print, colored or poor quality illustrations and
photographs, print bleed-through, substandard margins, and improper
alignment can adversely affect reproduction.

In the unlikely event that the author did not send a complete manuscript
and there are missing pages, these will be noted. Also, if unauthorized
copyright material had to be removed, a note will indicate the deletion.

UMI®

UMI Microform 1439967
Copyright 2007 by ProQuest Information and Learning Company.
All rights reserved. This microform edition is protected against
unauthorized copying under Title 17, United States Code.

ProQuest Information and Learning Company
300 North Zeeb Road
P.O. Box 1346
Ann Arbor, MI 48106-1346

UNLV
UNIVERSITY OF NEVADA LAS VEGAS

Thesis Approval
The Graduate College
University of Nevada, Las Vegas

JULY 14   , 2006

The Thesis prepared by

_____April Dianne Azouz_____

Entitled

EVIDENCE OF AN ACTIVE ENSO AND PDO DURING THE MID-HOLOCENE FROM

_____A COSTA RICAN SPELEOTHEM_____

_____

is approved in partial fulfillment of the requirements for the degree of

_____MASTERS   IN GEOSCIENCE_____

_____
Examination Committee Chair

_____
Dean of the Graduate College

_____
Examination Committee Member

_____
Examination Committee Member

_____
Graduate College Faculty Representative

1017-53   ii

ABSTRACT

Evidence of an active ENSO and PDO during the mid-Holocene from a Costa Rican speleothem

by

April D. Azouz

Dr. Matthew Lachniet, Examination Committee Chair
Professor of Geoscience
University of Nevada, Las Vegas

The El Niño/Southern Oscillation (ENSO) and the Pacific Decadal

Oscillation (PDO) are the most important sources of interannual to

multidecadal climate variability in the tropics. A high resolution (~3.8

years/sample) paleoclimate record of Central American rainfall variability

has been reconstructed from a U/Th-dated stalagmite (7890 to 6490 yrs

B.P.) from Costa Rica to constrain the onset and variability of ENSO

throughout the Holocene, and to determine its role in generating regional

climate anomalies. I suggest drier conditions, forced by El Niño and/or

the PDO, are represented by higher $\delta^{18}O$ values, and are correlative with

higher $\delta^{13}C$ values, indicating that soil respiration rates are affected by

regional climate variability, which are recorded in the speleothem

stratigraphy grayscale values. This study provides new evidence, based

on 3 different proxies, that throughout the middle Holocene, rainfall was

varying at interdecadal timescales, which I attribute to low frequency
variability in ENSO and the PDO.

iv

TABLE OF CONTENTS

LIST OF FIGURES

ACKNOWLEDGEMENTS

CHAPTER 1

INTRODUCTION

Purpose of Study

The development of high quality Holocene paleoclimate records

throughout the tropical Pacific is crucial to our understanding of the

driving forces that produce the two dominant modes of Pacific climate

variability: the El Niño Southern Oscillation (ENSO) and the Pacific

Decadal Oscillation (PDO). The tropics receive the greatest amount of

solar radiation, and as the 'heat engine' for global circulation are

responsible for driving atmospheric and oceanic circulation to higher

latitudes. Few quantitative terrestrial isotopic paleoclimatic studies exist

for this part of the world, therefore, understanding tropical climate

history is important because it provides information for ENSO and PDO

predictive climate modeling and future water use planning in Central

America.

Many studies throughout the Pacific basin suggest that the Holocene

is characterized by an increase in ENSO frequency and amplitude

towards the present since the mid-Holocene (Moy et al., 2002; Tudhope

et al., 2001; Cole, 2001; Rodbell et al., 1999). The middle Holocene is of

1

special interest because various proxy records and modeling studies suggest that ENSO was suppressed/weakened during this period (Otto-Bleisner,1999; Tudhope et al., 2001; Clement et al., 2000; Koutavas et al. 2002), and only between 7000-5000 years B.P. did the onset of modern ENSO conditions begin (Moy et al. 2002; Rodbell et al., 1999; Sandweiss et al., 2001). Not all regions are affected by tropical Pacific climate variability in the same manner and magnitude, therefore knowledge of the stability of teleconnections between Costa Rica and other regions directly affected by ENSO and the PDO during the Holocene will help elucidate how the tropics respond to climatic shifts and variations in moisture availability.

Tropical climate change is reflected in speleothem carbonate because oxygen isotope variations reflect the amount of rainfall. Speleothems are cave calcite deposits that incorporate rainfall derived oxygen into their precipitated calcite, and can be precisely dated by U-series isotopes (Richards and Dorale, 2003). In this study, a speleothem is used as a paleoclimate proxy to determine the role of ENSO and the PDO in generating regional climate anomalies in Costa Rica throughout the middle Holocene.

Costa Rica is located between 9-11° N and is found at almost the narrowest point on the Central American isthmus (Figure 1.1). Costa Rica is segmented by high cordilleras, therefore, the oceanic and climatological affects on Costa Rica are produced from both the Pacific

2

Ocean and Caribbean Sea (Waylen et al., 1996). Costa Rica is an important area to document the speleothem isotope record because it is a region directly affected by Pacific climate variability and should provide a reliable record to track changes in the migration of the Intertropical Convergence Zone (ITCZ). During El Niño events and the positive phase of the PDO, drier conditions throughout Costa Rica are produced (Waylen et al., 1996) due to an increase in SSTs across the equatorial Pacific Ocean, which displaces the ITCZ further south. Costa Rica is a key region affected by ENSO and the PDO, therefore, paleoclimate records generated there should reflect ENSO and PDO history.

The goal of this study is to determine the role of Pacific climate variability, ENSO and the PDO, in Central America throughout the mid-Holocene. A high resolution rainfall proxy based on oxygen isotope ($\delta^{18}O$) variations has been reconstructed from a Costa Rican speleothem. The amount effect is the dominant control on $\delta^{18}O$ variations, therefore during El Niño events and the warm phase of the PDO, drier conditions with higher $\delta^{18}O$ values should be recorded in speleothem carbonate.

Carbon isotope ($\delta^{13}C$) variations, combined with $\delta^{18}O$ as a rainfall proxy, were analyzed to address the relationship between tropical rainfall and biological respiration. Carbon isotope values in speleothems are dependent on the photosynthetic pathway of overlying vegetation (Dorale et al., 1998; Richards and Dorale, 2003), soil respiration, soil/water rock equilibration time (Baker et al., 1997), and climate (Burns et al., 2002).

3

Grayscale stratigraphic analysis was also performed, and provides an ultra high resolution record of the internal speleothem stratigraphy, resulting in three time series which will be compared to establish a climate proxy that can be used to resolve rainfall variability and carbon cycling within the soil zone, overlying limestone bedrock, and atmospheric CO_2, over the interval of speleothem growth.
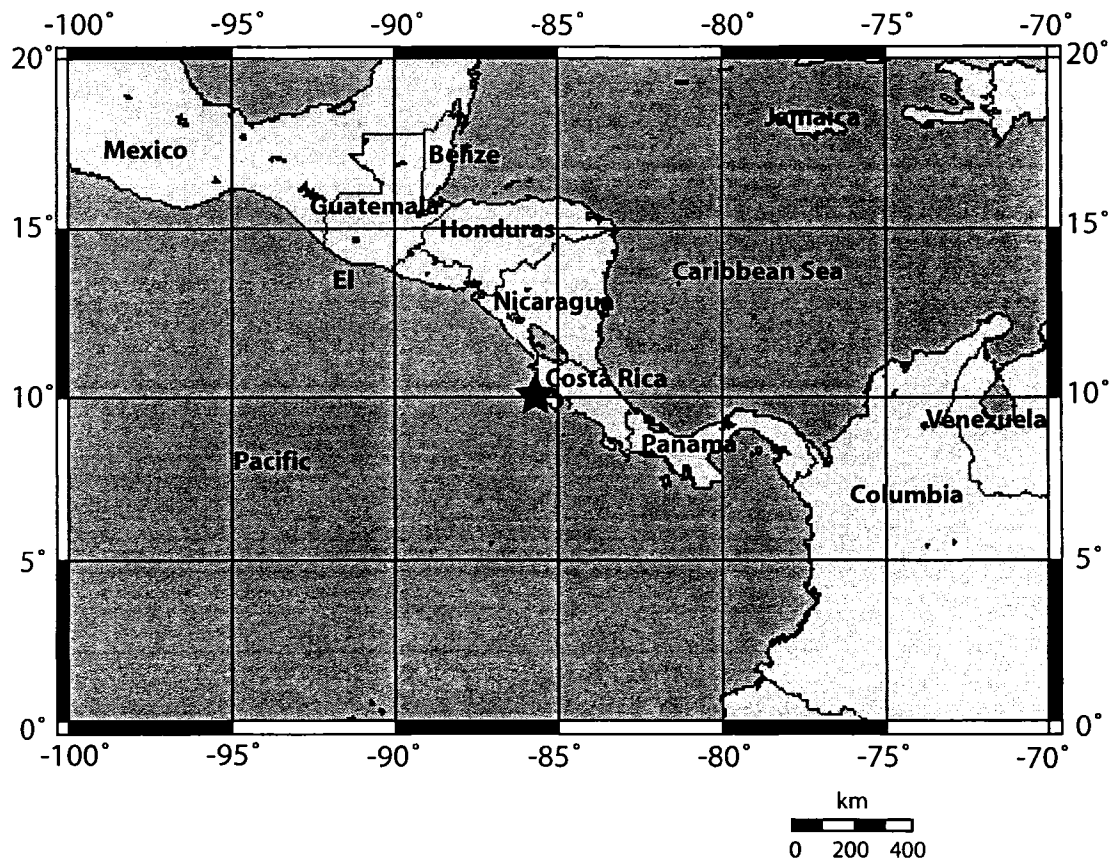
Figure 1.1. Map of Central America. Star indicates location of field area in Barra Honda National Park in Costa Rica

5

CHAPTER 2

BACKGROUND

Geological Background

During the Pliocene, the convergence of the Caribbean plate with the

Cocos and Nazca plates produced the Isthmus of Panama, which

includes Costa Rica and Panama (Duque-Caro, 1990). The oldest rocks

found in Costa Rica are the ophiolitic Late Mesozoic Nicoya Complex,

which are Jurassic to Upper Cretaceous sea floor rocks (Mora, 1992;

Castillo-Munoz, 1983). Since the late Mesozoic, several tectonic events

have accreted, faulted, uplifted, and allowed deposition of oceanic and

neritic sediments (Mora, 1992). The Rivas formation, which consists

primarily of interbedded mudstones and siltstones, directly overlies the

Cretaceous ophiolite sequence.

During the Eocene, the Barra Honda formation, consisting of shallow

water reef limestones, were later uplifted above sea level and commonly

show evidence of karstic features (Figure 2.1). Barra Honda National

Park, which is one of the best known and best developed areas of karst

in Central America, is located in the Tempisque Basin where the Nicoya

Peninsula joins the mainland (Figure 2.2). The maximum thickness of

6

the Barra Honda formation is ~250 m and it is not overlain by any other unit, suggesting that continuous uplift of this region occurred since deposition during the Eocene (Mora, 1992).

Terciopelo cave, which is where sample CT-7 was collected, is one of the many caves located in Barra Honda National Park. Barra Honda presently receives ~1.5 m of rain each year (Coen, 1983) and the mean monthly temperature in the Guanacaste dry forest was 28°C for the period between 1960-1970 (Gordon et al., 1974).

Cave and Speleothem Formation

Unsubmerged limestone caves provide a favorable environment for speleothem calcite deposition, which precipitates from dripwaters entering the cave from the land surface above (e.g. White, 2004). Speleothem formation results from rainfall percolating through the soil zone. As rainwater infiltrates the soil, biological respiration increases the pCO_2, which is higher than the pCO_2 in the atmosphere. This soil moisture is charged with the biogenic CO_2, which increases the acidity of water by the formation of carbonic acid. Water infiltrates downward until it reaches the carbonate bedrock, where it percolates through fractures within the limestone, dissolving the calcite until reaching calcite saturation. Upon reaching a pre-existing cave with atmospheric pCO_2 concentrations, calcite saturated groundwater will degas CO_2 (Hendy, 1971), resulting in precipitation of solid calcite speleothems

7

(Figure 2.3). Paleoclimate information, in the form of $\delta^{18}O$ and $\delta^{13}C$ values are also preserved within the calcite structure of the speleothem (Gascoyne, 1992).

The internal speleothem stratigraphy can display varying degrees of color and intensity when viewed in both reflected and ultraviolet light (Van Beynen et al., 2001), and can provide paleoclimate information in combination with stable isotope analysis. Speleothems fluoresce due to the presence of organic acids trapped within the calcite (Gascoyne, 1977), varying concentrations of trace elements (James, 1997), and can result from differences in porosity of individual layers, driven by infiltration and dripwater rate (Genty, 1992). Luminescent laminations are dependent on surface climate, soil/ vegetation characteristics, and groundwater hydrology at the site (Baker et al., 1999), therefore, the internal speleothem stratigraphy provides an excellent paleoenvironmental proxy.

Oxygen and Carbon Isotopes

Isotopes are used as tracers of certain geochemical processes, such as evaporation, precipitation, and photosynthesis. An isotope is an atom with the same number of protons and a different number of neutrons located in its nucleus. Isotopes of an element have identical chemical properties, but differ in their masses. Isotopic fractionation occurs due

8

to the difference in masses, in which certain geochemical processes prefer either the heavier or lighter form of that element.

Isotopic values are reported as ratios expressed in delta (δ) notation where R= $^{18}O/^{16}O$ or $^{13}C/^{12}C$, expressed in per mil (‰) notation with respect to two standards: Vienna PeeDee Belemnite (VPDB) for calcite, and Vienna Standard Mean Ocean Water (VSMOW) for water.

$$\delta\ (‰) = \frac{R_{sample} - R_{standard}}{R_{standard}} \times 1000$$

where R= $^{18}O/^{16}O$ or $^{13}C/^{12}C$

Many factors contribute to the $\delta^{18}O$ values of speleothem calcite. The average $\delta^{18}O$ values of rainfall may reflect the temperature of condensation, seasonality of precipitation, ice volume effect, continental effects, sources of water vapor and the amount effect (Dansgaard, 1964; Harmon et al., 1978). The air temperature in Costa Rica does not vary more than a few degrees annually, and within a cave system, temperature variations are dampened relative to the atmospheric temperature. Variations in $\delta^{18}O$ values due to temperature dependent fractionation are likely to be constant, because at ~25°C, cave temperature variations of ~1°C should result in only a 0.25‰ effect on $\delta^{18}O$ values of speleothem calcite precipitating in isotopic equilibrium with drip waters (Kim and O'Neil, 1997). Also, in poorly ventilated tropical caves, such as Terciopelo cave, where relative humidity is near 100% year-round, kinetic fractionation from evaporation should be minimal.

9

In the tropics, variations in $\delta^{18}O$ values of rainfall indicate changes in the amount of precipitation due to the 'amount effect' (Dansgaard, 1964), in which the initial rainfall is enriched in ^{18}O isotopes, while further precipitation becomes increasingly depleted in ^{18}O isotopes (Dansgaard, 1964; Rozanski, 1993; Lachniet and Patterson, 2003, 2006) (Figure 2.4). Kinetic fractionation caused by rapid CO_2 degassing, rapid calcite precipitation and cave-water evaporation may also affect the $\delta^{18}O$ and $\delta^{13}C$ values of stalagmite carbonate (Mickler et al., 2004). In tropical regions, the most likely source of kinetic fractionation would be due to rapid degassing of CO_2 from carbonate-saturated drip waters, and not from evaporation of water (McDermott, 2004), due to the high relative humidity within the cave system. Evaporation within the soil zone could affect the $\delta^{18}O$ values of speleothem calcite and would increase the $\delta^{18}O$ value of drip water before reaching the stalagmite (Lachniet et al., 2004a). Rapid CO_2 degassing produces an enrichment in $\delta^{18}O$ values, which results in a shift in the $\delta^{18}O$ values in the same direction as the amount effect (Burns et al., 2002). For example, rapid degassing produces higher $\delta^{18}O$ value, similarly to the amount effect, where drier conditions produce higher $\delta^{18}O$ values. Therefore, kinetic fractionation due to rapid degassing or evaporation within the soil zone, leads to an increase in the $\delta^{18}O$ values of the speleothem calcite.

Many factors influence speleothem $\delta^{13}C$ values. The carbon isotope composition of speleothems can be used to infer the isotopic composition

of atmospheric CO_2 (Baskaran and Krishnamurthy, 1993), type of vegetation overlying the cave (Dorale et al., 1992), contribution of soil carbon relative to aquifer limestone, the dissolved inorganic carbon (DIC) content of the dripwater, and climate (Burns et al., 2002). Dry tropical rainforest vegetation, which is located throughout Barra Honda National Park, is dominated by C_3 plants, which produce $\delta^{13}C$ values in speleothems to have a range between -14 to -6‰ VPDB. Plants that utilize the C_4 pathway, such as warm season grasses and maize, exhibit higher $\delta^{13}C$ values and produces speleothem $\delta^{13}C$ values between -6 to +2‰ VPDB. In environments where the soil-water residence time is short, complete isotopic equilibration between soil CO_2 and infiltrating water may not occur, resulting in water containing an isotopically heavier atmospheric CO_2 component (McDermott, 2004).

Kinetic fractionation processes, such as evaporation, rapid CO_2 degassing, and prior calcite precipitation would enrich the $\delta^{13}C$ values of the precipitated calcite. To determine the effects of equilibrium versus kinetic fractionation of tropical speleothems, Mickler et al. (2004) analyzed drip water samples, $CaCO_3$ precipitated on glass plates, and speleothem $\delta^{18}O$ and $\delta^{13}C$ values. Although speleothems may appear to precipitate in isotopic equilibrium, Mickler et al. (2004) concluded that kinetic fractionation effects most likely are occurring, which can increase or decrease the $\delta^{13}C$ values. Precipitation of calcite in isotopic equilibrium is assumed to occur when cave environments have high

11

relative humidity, which is an assumption that must be made in order to use $\delta^{18}O$ and $\delta^{13}C$ values of speleothems as a paleoclimate proxy.

Climatological Background

The two dominant factors that control intra- and inter-annual precipitation throughout much of Central America are the annual migration of the Intertropical Convergence Zone (ITCZ) and ENSO (Waylen et al., 1996). The ITCZ is a zone of low pressure that occurs where the Northeast and Southeast trade winds converge at ~5-10° N, resulting in a band of heavy precipitation. The ITCZ migrates seasonally following the most intense solar radiation and the warmest sea surface temperatures (SSTs) to reach ~12° N in August and recede to its southernmost position in February (Coen, 1983).

The annual migration of the ITCZ results in wet and dry seasons in the tropics, and together with seasonal changes in wind direction, is referred to as the Central America Monsoon (Giannini et al., 2000). The wet season in Costa Rica commonly starts in May and lasts through November, while the dry season occurs from December to April (Coen, 1983). Although rain can occur in the dry season, ~70% of the annual precipitation falls during the wet season (Coen, 1983).

The El Niño/Southern Oscillation (ENSO) also affects Costa Rican climate. There is a strong link between ENSO events and large-scale precipitation patterns (Ropelewski and Halpert, 1987). ENSO events

12

occur from the complex interaction between the ocean and atmosphere. ENSO refers to tropical Pacific Ocean variability, including both El Niño and La Nina events. El Niño warm events disrupt normal atmospheric and oceanic circulation, which produces anomalous weather patterns throughout the world every 2-7 years (Enfield and Cid, 1991). El Niño modulates the annual migration of the ITCZ by displacing it further south near South America. This prolongs the dry season of El Niño and produces drought on the Pacific Coast drainage of Costa Rica (Waylen et al., 1996).

During an El Niño year, a warm tongue of water spreads eastward along the equator due to a weakening of the trade winds and produces large changes in atmospheric circulation (Figure 2.5). Above average SSTs in the Eastern Equatorial Pacific during El Niño years can induce an early dry season through much of southern Central America (Enfield and Alfaro, 1999). When SSTs are elevated for five or more consecutive months, an El Niño warm phase is generated. The warm phase is associated with lower mean annual precipitation over much of the equatorial Americas (Waylen et al., 1996; Vuille et al., 2003). During a La Niña year, the opposite occurs, in which a cool tongue spreads eastward along the equator due to a strengthening of the trade winds and increases rainfall on the Pacific slope of Costa Rica and decreases rainfall on the Atlantic slope.

13

Similarly to ENSO, the Pacific Decadal Oscillation (PDO) is a long-lived El Niño-like pattern of Pacific climate variability (Mantua and Hare, 2002) (Figure 2.6). Three main characteristics distinguish the PDO from ENSO. First, 20th century PDO events occur on longer timescales (20-30 years) (Mantua and Hare, 2002) compared to ENSO events (2-7 years) (Enfield and Cid, 1991). Second, the primary effects of the PDO occur in the extratropics, more specifically in the North Pacific, with secondary climatic effects in the tropics. However, ENSO primarily affects the tropics with teleconnections to the extratropics occurring later. Third, while the causes for ENSO variability are relatively well-understood, the causal mechanisms for the PDO remain unclear (Mantua and Hare, 2002).

The PDO varies from warm to cool phases, similarly to ENSO. During warm PDO phases, SSTs are anomalously cool in the central North Pacific with anomalously warm SSTs along the west coast of North America. Sea level pressure (SLP) in the northern North Pacific is low, causing enhanced counterclockwise (cyclonic) winds. High SLP occurs over the northern subtropical Pacific, causing enhanced clockwise (anticyclonic) winds. The cool phases of the PDO are opposite of those associated with the warm PDO phases (Mantua and Hare, 2002). Temporally, the PDO fluctuates between common periodicities in the 15-25 year and 50-70 year bands (Minobe, 1999). PDO variability demonstrates that "normal" climate conditions can vary, resulting in

14

climate anomalies that can persist on decadal to multi-decadal time periods. The PDO is dependent on ENSO variability on all time scales (Newman et al., 2003); therefore, it is their interaction that determines interannual variability of the tropical Pacific (Lluch-Cota et al., 2001).

Previous Work

Although the instrumental record of tropical climate is only present for the past ~150 years, various proxy records throughout the tropical Pacific record past ENSO events during the Holocene, which indicate variable intensities and recurrence intervals (e.g. Sandweiss et al., 2001). Rodbell et al. (1999) and Moy et al. (2002) used sediment cores from an alpine lake in Ecuador that contains clastic laminae deposits that directly correlate with historical El Niño events. They suggested that interannual ENSO variability was dramatically weaker prior to ~7000 years B.P as shown by the increase in frequency of the clastic laminae deposits after 7000 yrs B.P.

Corals can record seasonal to annual resolution (Gagan et al., 2000) and are excellent paleoclimate proxies. The stable isotopic composition of corals can extend the instrumental record of tropical climate back to the late Quaternary (Charles et al., 2003). Since corals only grow in warm tropical waters and ENSO is focused primarily in the tropics, corals record annual to monthly variations and can produce long-term ENSO records relative to the historical record of ENSO. Corals from the tropical

15

Pacific have been the focus of many paleoclimate studies due to the importance of ENSO in global climate variability (Gagan et al., 1999). However, high resolution coral records are often discontinuous and of short duration (Cole et al., 1993). A further problem is that corals may bleach during very warm El Niño events, which could alter the original isotopic signature (Linsley et al, 1994).

ENSO paleoclimate records based on speleothems can complement those derived from corals (Lachniet et al., 2004; Brooks et al., 1999). Most speleothem-based paleoclimate reconstructions rely upon oxygen isotopic measurements of speleothem calcite or upon thickness of annual growth bands (e.g., Fleitmann et al., 2004) because oxygen isotopes from tropical speleothems provide a detailed rainfall record relating to ENSO. For example, to better predict the Indian Monsoon and its link to ENSO, Fleitmann et al. (2004) analyzed three stalagmites from Southern Oman which provided a detailed Indian Ocean monsoon rainfall record for the past 780 years. Lachniet et al. (2004) generated a high resolution $\delta^{18}O$ rainfall record from the Isthmus of Panama to determine the influence ENSO has on generating regional hydrologic anomalies. Speleothems collected from locations surrounding the Pacific Ocean, and throughout the world, can generate high resolution long-term records of ENSO variability throughout the Holocene.

To illustrate the long-term trends in the PDO, several studies have used proxy evidence to demonstrate PDO-related climate change. A

16

dendrochronology study reconstructed for North American air temperature since 1600 A.D., demonstrated the 50-70 year PDO periodicity throughout the entire record (Fritts, 1991; Minobe, 1997). The Sr/Ca variability in long-lived corals from the western tropical Pacific show a strong PDO signal in the extracted SST history (Linsley et al., 2000), suggesting that robust teleconnections to the tropics and the southern hemisphere exist (Evans et al., 2000).

N

600
400
200
0

Cerro Barra Honda
Terciopelo

Cerro Corralillo

Rio Nacaome

600
400
200
0

0   500   1000
meters

Limestone: Barra Honda Formation (Eocene)

Interbedded siltstone and mudstone: Rivas Formation
(Paleocene)

Ophiolite Sequence (not shown): Nicoya Complex
(Jurassic-Cretaceous)
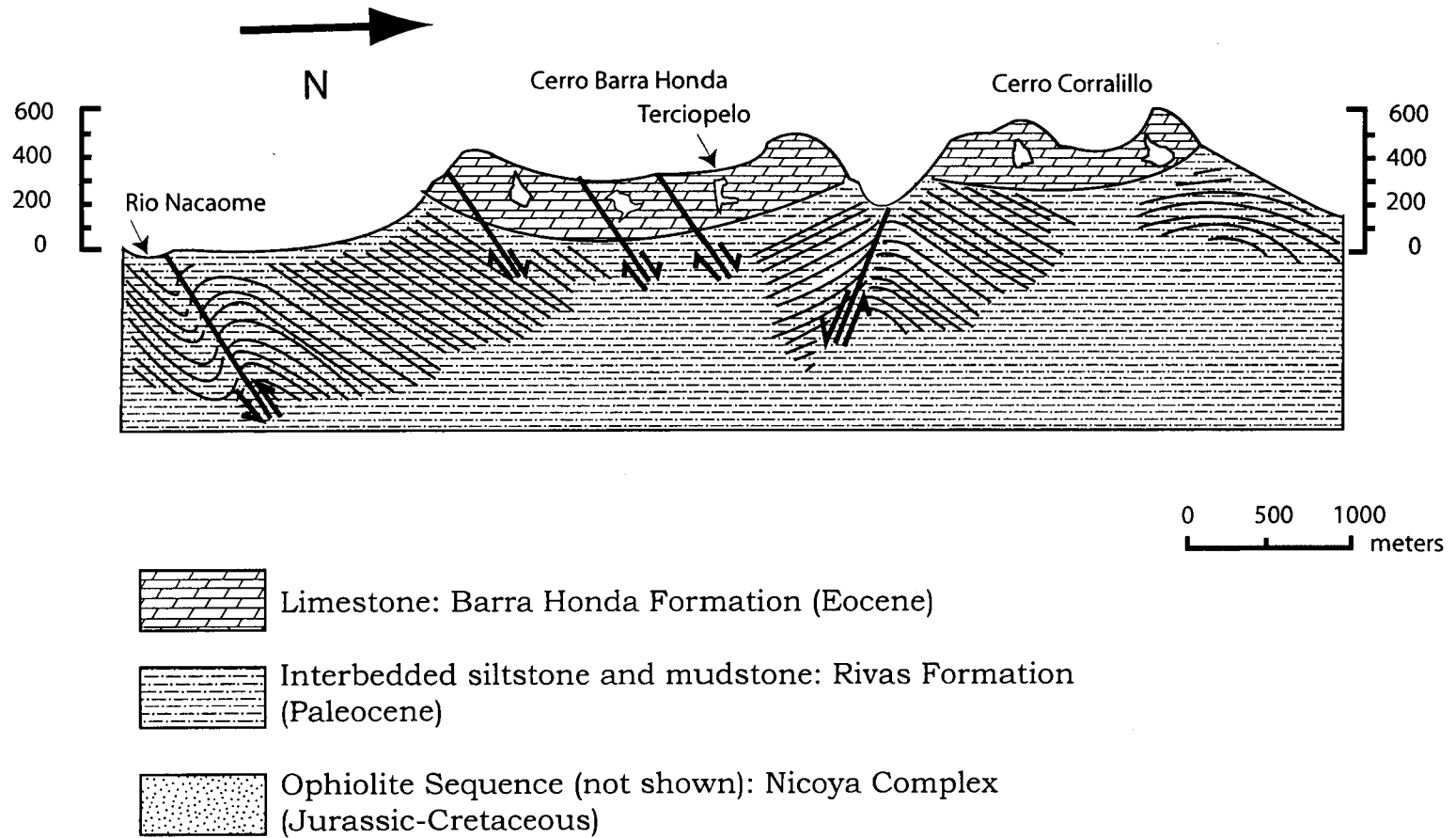
Figure 2.1. Cross-sectional view of Barra Honda National Park. Stratigraphically, the oldest unit is the Nicoya complex, although it is not visible in Barra Honda National Park. Black lines overlying the Rivas Formation illustrate folded beds. Adapted from Mora Castro, 1981.
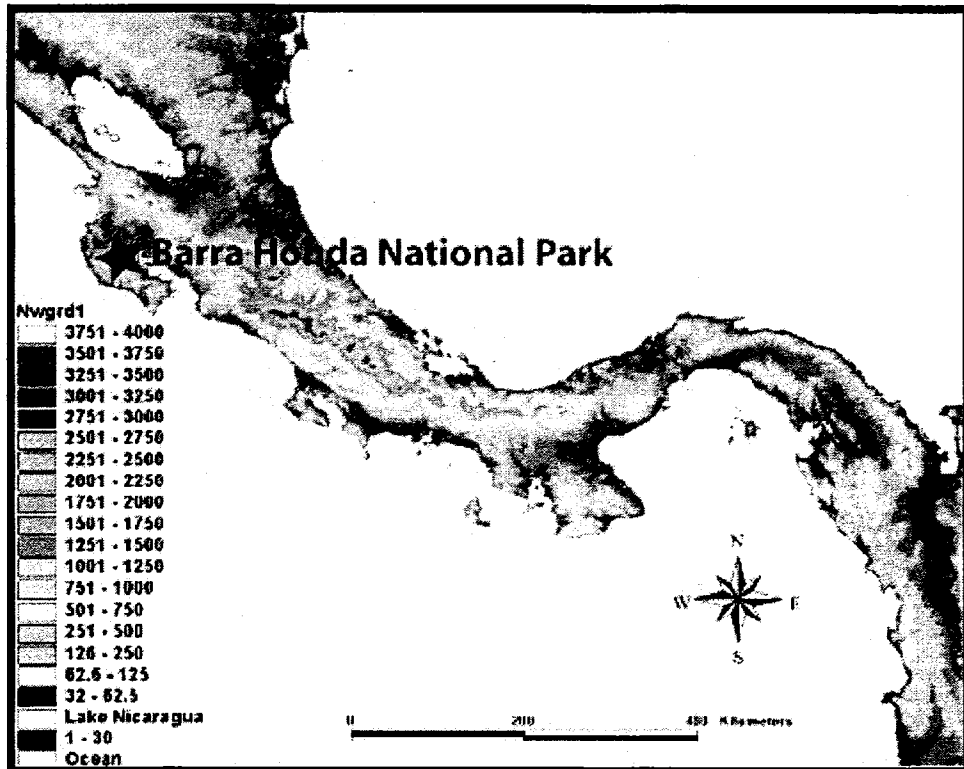
Figure 2.2. Digital Elevation Model of southern Central
America. The star represents Barra Honda National Park
located on the Nicoya Peninsula of Costa Rica. The DEM source
is the USGS GTOPO30 data set US Geological Survey (1996).

19
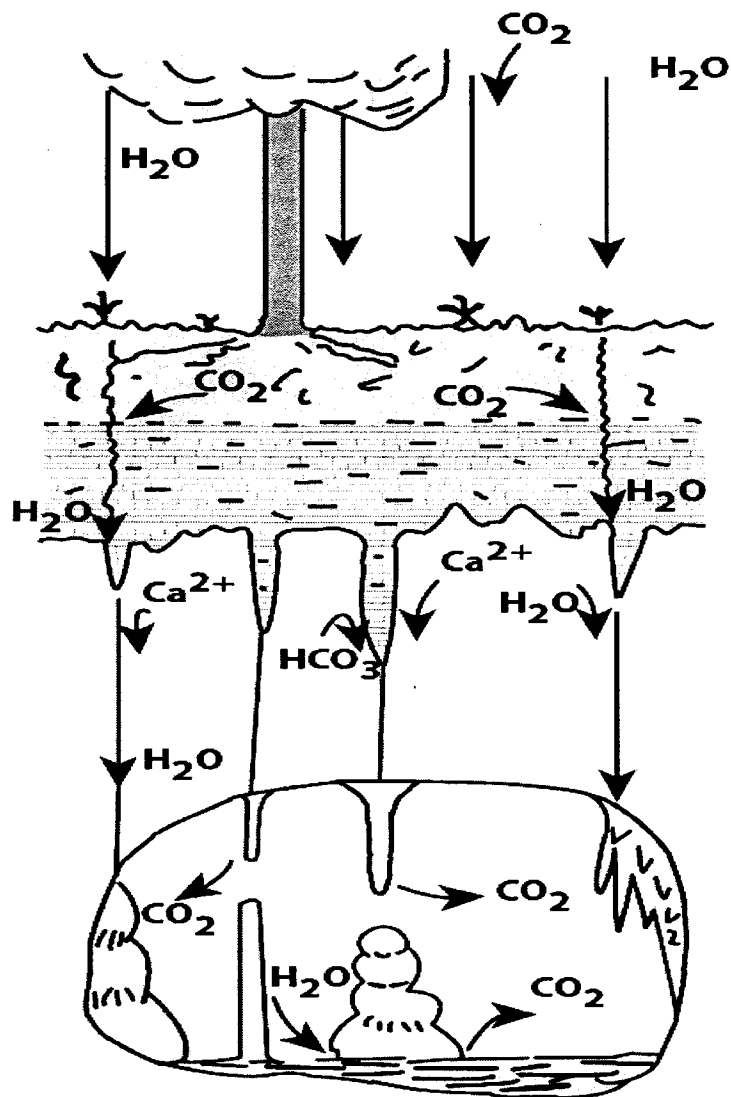
Figure 2.3. Schematic diagram illustrating cave formation processes. Water infiltrates through the soil zone where biological respiration increases pCO_2 in the soil, and increases the acidity of the infiltrating water. As water reaches the limestone bedrock, it dissolves the limestone until saturation. Once the water reaches a preexisting cave with lower pCO_2, CO_2 degasses and calcium carbonate precipitates out of solution. Modified from Holland et al., 1964.

20
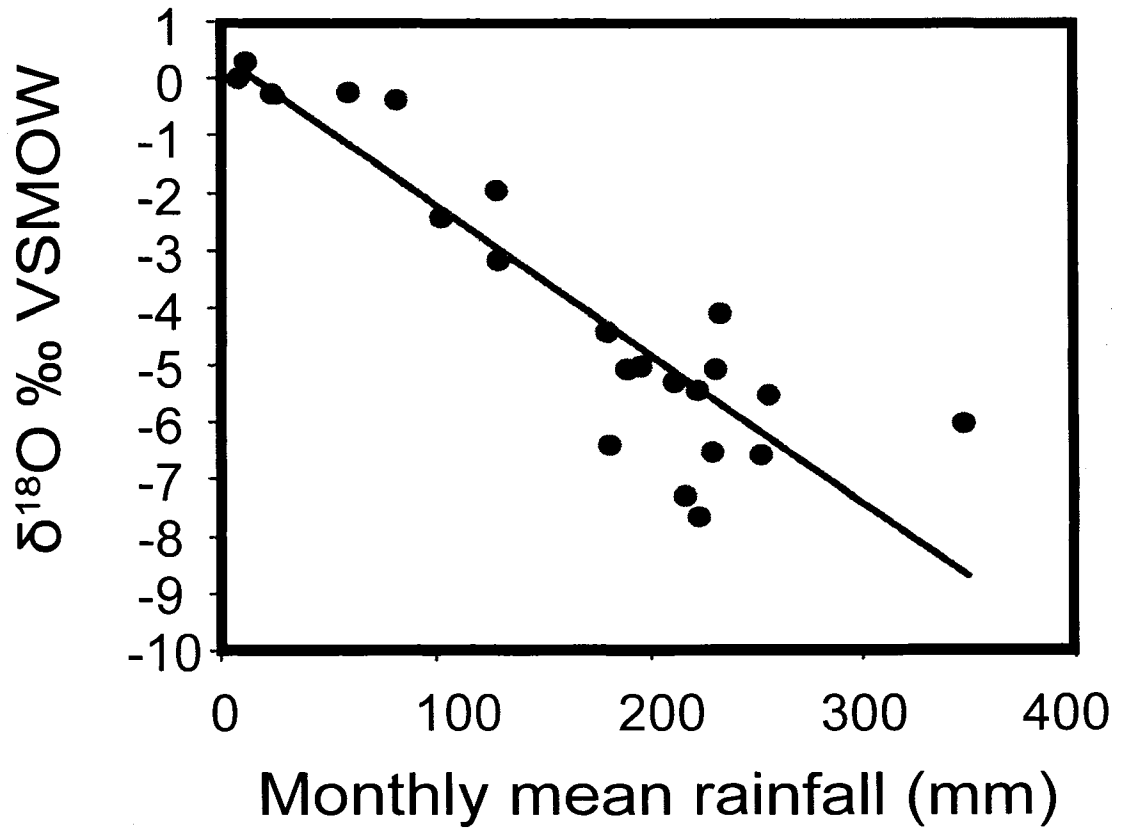
Figure 2.4. The amount effect of rainfall in Panama and Costa Rica. From Lachniet et al. 2004.

21

A.)

Normal conditions

El Niño Conditions

B)
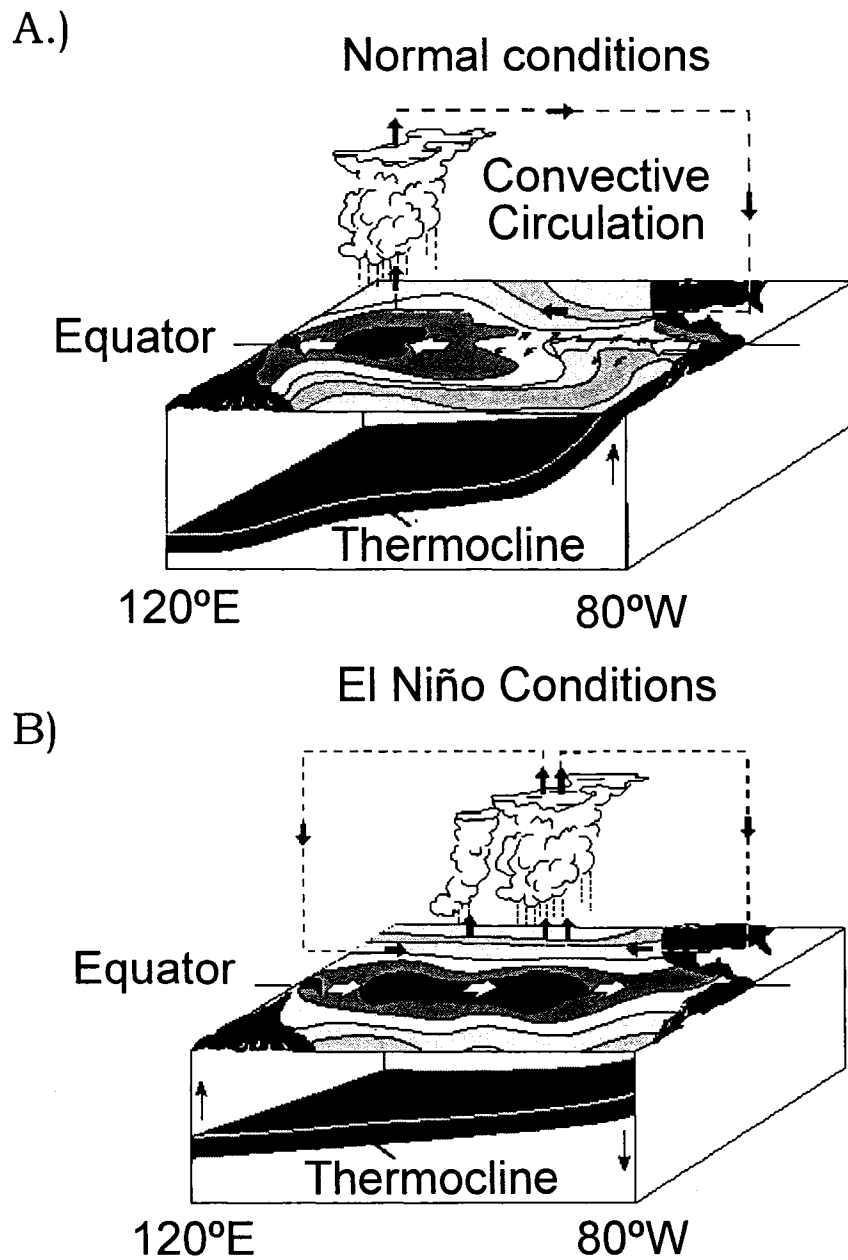
Figure 2.5. Schematic diagrams comparing A) normal conditions of the tropical Pacific and B) El Niño conditions. Modified from http://www.elnino.noaa.gov/.

22

Pacific Decadal Oscillation

positive phase

negative phase

0.8

0.4

0.2

0.0

-0.2

-0.6
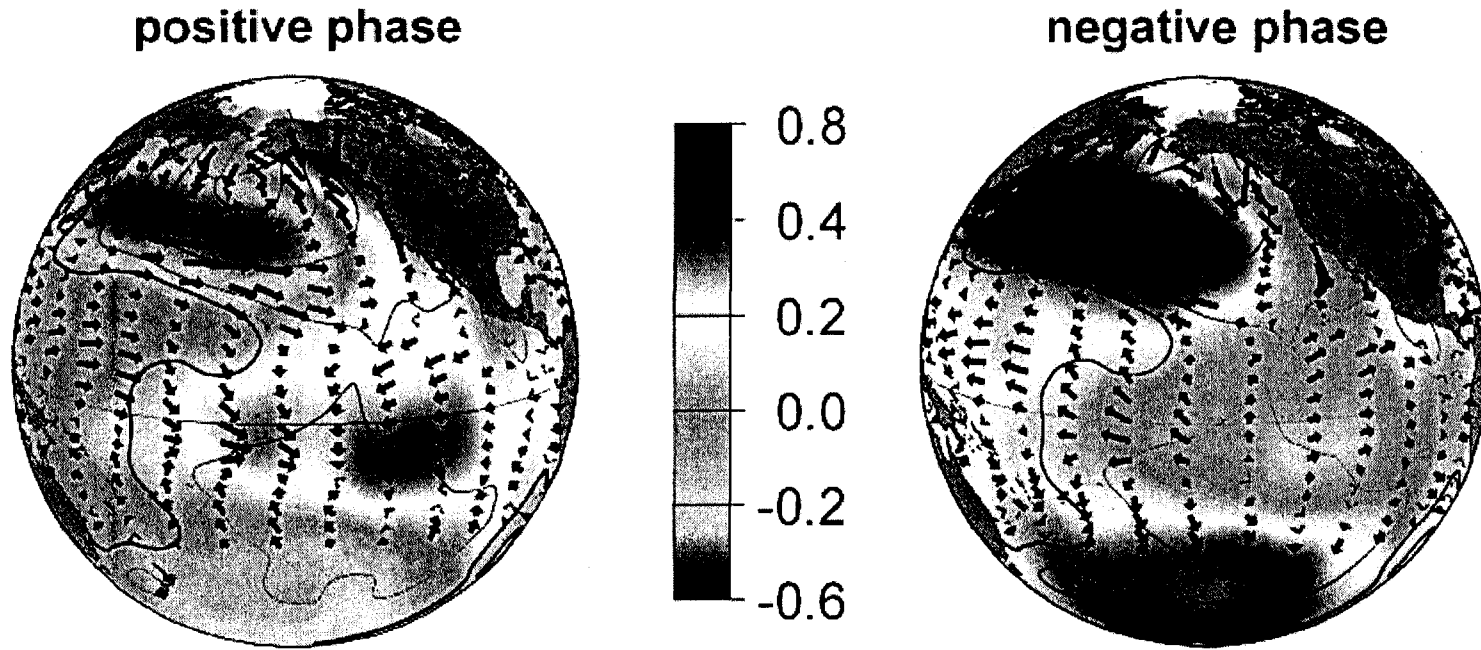
Figure 2.6. The Pacific Decadal Oscillation during its positive and negative phases. The colors represent sea surface temperatures (SST), the contours represent sea level pressure (SLP), and the vectors represent surface wind stress anomaly patterns. From http://jisao.washington.edu/pdo/

CHAPTER 3

METHODS

Sample Collection

Stalagmite CT-7, which is ~37cm long along the growth axis (Figure 3.1), was collected from Terciopelo cave in Barra Honda National Park. The entrance to Terciopelo cave is a vertical shaft with a ~17 m drop onto an inclined surface that descends ~39 m below the surface to the back of the cave (Figure 3.2). Sample CT-7 was collected in January of 2004 and was removed from a constricted, poorly ventilated passage approximately ~25 m laterally and ~50 m vertically from the cave entrance. Within the cave system, no streams were present. At the sample location in March 2005, the temperature was 26-27° C and the relative humidity was 94-97%.

Sample Preparation

Sample CT-7 was halved along the growth axis. The surface was polished to reveal an interior of white and clear calcite with visible sub-millimeter layers of calcite of varying density. Thin sections were made

24

sequentially, from the base to the tip, to analyze and identify any possible hiatuses, inclusions, and detritus within the calcite. By illuminating sample CT-7 with ultraviolet light, the internal speleothem stratigraphy is displayed in greater detail, which allowed for more accurate drilling within single layers, and provided more confidence in the age calculated with U-series dating.

Stable Isotope Sampling

Calcite subsamples were drilled from the cut and polished speleothem surface at 1mm intervals along the growth axis to sample for oxygen and carbon isotopes. Using a Sherline™ drill press model 5410, fitted with a 0.5mm drill bit, 374 calcite subsamples of ~100 µg were extracted and analyzed for oxygen and carbon isotopic ratios using a Finnigan Delta +XL ratio mass spectrometer with dual inlet system coupled to a Kiel III automated carbonate preparation device. This work was performed at the University of Massachusetts stable isotope laboratory.

Radiometric Dating

Sixteen calcite subsamples of ~400 mg were removed, along growth bands, from sample CT-7 for U/Th analysis at the University of New Mexico Radiogenic Laboratory. Four calcite subsamples were removed along an individual growth band, at four different locations throughout CT-7, to produce one weighted average age per growth band.

25

Chemical separations were performed to purify and separate uranium from thorium according to a modified version of the procedures followed by the isotope lab at the University of Minnesota as described by Polyak and Asmerom (2001). Calcite powders were transferred to pre-weighed 30 ml teflon vials and reweighed. The samples were covered with deionized water and then dissolved in 15N HNO_3. Once dissolved, the samples were spiked with ~1g of a solution containing known concentrations and isotopic composition of ^{236}U, ^{233}U, and ^{229}U and then the solution was dried on a hot plate. Then, a few drops of deionized water and perchloric acid were added to the samples and re-dissolved in a few drops of 15N HNO_3 and dried. The U and Th are co-precipitated with Fe by adding NH_4OH, until Fe coagulates and precipitates. The mixture is centrifuged and the supernatant discarded. The solution is re-dissolved in 15N HNO_3, transferred back to the clean 30 ml Teflon vial, dried and re-dissolved twice in 15N HNO_3. The sample is dissolved again in 7N HNO_3 and loaded on an anion exchange column to separately extract purified U and Th fractions. For a more detailed description of chemical separations and procedures, see Appendix I.

Measurements were made on a Micromass Sector 54 Thermal Ionization Mass Spectrometer (TIMS) with a WARP filter. It has seven Faraday cups and an ion-counting Daly multiplier. Samples were loaded onto filaments using the graphite sandwich method in which the sample

is loaded onto the center of the filament between two layers of graphite in order to amplify ionization efficiency.

Speleothems can be dated by the ^{238}U- ^{234}U- ^{230}Th disequilibrium techniques (Dorale et al., 2004). Uranium series dating is based on the fractionation of parent U isotopes (^{238}U, ^{235}U and ^{234}U) from their long-lived daughters ^{231}Pa and ^{230}Th. The ^{238}U decay series, and the $^{234}U/^{230}Th$ ratio of a sample can be used to determine the time since carbonate deposition in karst environments (Richards and Dorale, 2003). Uranium is soluble in water and therefore is mobilized in the meteoric environment. In typical groundwater, uranium combines with water to form the uranyl ion (UO_2^{+2}) which is stable in carbonate complexes (Gascoyne 1992b). In contrast, thorium is insoluble and is essentially left behind, and is either precipitated or adsorbed onto detrital particulates (Richards and Dorale, 2003). Therefore, during the formation of secondary calcite deposits, such as speleothems, uranium is co-precipitated with the $CaCO_3$, while the immediate daughter products (^{230}Th) is absent. This form of disequilibrium occurring in speleothem deposition is referred to as the daughter- deficiency method (Richards and Dorale, 2003).

The general equations used in determining the age of speleothems assume that all ^{230}Th present was formed *in situ* by radioactive decay of the co-precipitated U. For pure authigenic calcite or aragonite, the thorium content at the time of formation can be negligible, although,

allochthonous material, such as detrital clays with a significant amount of Th can become cemented or occluded within the speleothems. Initial ^{230}Th can also be incorporated into the speleothems by being transported in the colloidal phase, attached to organic molecules, or as carbonate complexes in solution (Richards and Dorale, 2003).

The isochron methodology allows one to separately distinguish between the amount of ingrown radiogenic daughter and its initial abundance. To determine and accommodate for initial ^{230}Th, four separate isochrons were created by dating 3 to 5 subsamples along the same growth layer to determine the initial ^{230}Th/^{232}Th activity ratio. By comparing ^{234}U/^{232}Th and ^{230}Th/^{232}Th data for age equivalent carbonate, the initial ^{230}Th/^{232}Th can be estimated from the intercept of this straight line relationship (Richards and Dorale, 2003). In speleothems with clean calcite where ^{232}Th contamination is minimal, the effect of using the incorrect ^{230}Th/^{232}Th initial ratio will be negligible (Richards and Dorale, 2003). U-series dates are presented with a 2σ error based on an initial ^{230}Th/^{232}Th ratio of the global value, 4.4 × 10^{-6}, with an uncertainty of ± 50 % applied.

Grayscale Analysis

An ultraviolet luminescence record for CT-7 was obtained by taking high resolution digital images from the base to the tip and splicing them together to produce one high resolution digital image. The image was

28

converted from blue-scale to grayscale with Adobe Photoshop. No adjustments for color contrast, resolution, or filtering were done to the image. Using Scion, a National Institute of Health grayscale image processing program, a multi-line transect paralleling the growth axis was analyzed for grayscale values throughout the entire length of the sample. Values range from 0 to 255, with lower values indicating lighter layers, and higher values indicating darker layers.

Statistical Analyses

Statistical analyses of paleoclimate time series provides a synthesis of proxy data that enhances the understanding of trends in the data set. The proxy data is analyzed with mathematical techniques that allow us to interpret the data in terms of the underlying geological mechanisms and processes.

Spectral analysis decomposes the original data set into underlying sine and cosine functions of particular wavelengths to determine the strength (power) of a given signal and helps elucidate the physical processes which generate variability within the time series (Schulz and Mudelsee, 2002).

Spectral analysis using the Lomb-Scargle Fourier transform was performed on all three data sets: oxygen and carbon isotopes, and grayscale values using the REDFIT program (Schulz and Mudelsee, 2002). REDFIT is useful because it allows spectral analysis from

29

unevenly spaced time series without requiring interpolation (Schulz and Mudelsee, 2002).

Wavelet analysis was performed on the detrended and normalized time series, which takes basic spectral analysis a step further by localizing variations of power within a time series (Torrence and Compo, 1998). The wavelet transform decomposes a time series into time-frequency space, which helps determine both the dominant modes of variability and how those modes vary with time (Torrence and Compo, 1998). The advantage of wavelet analysis over a Fourier transform is that it allows time localization of statistically significant variance within a time series.

30
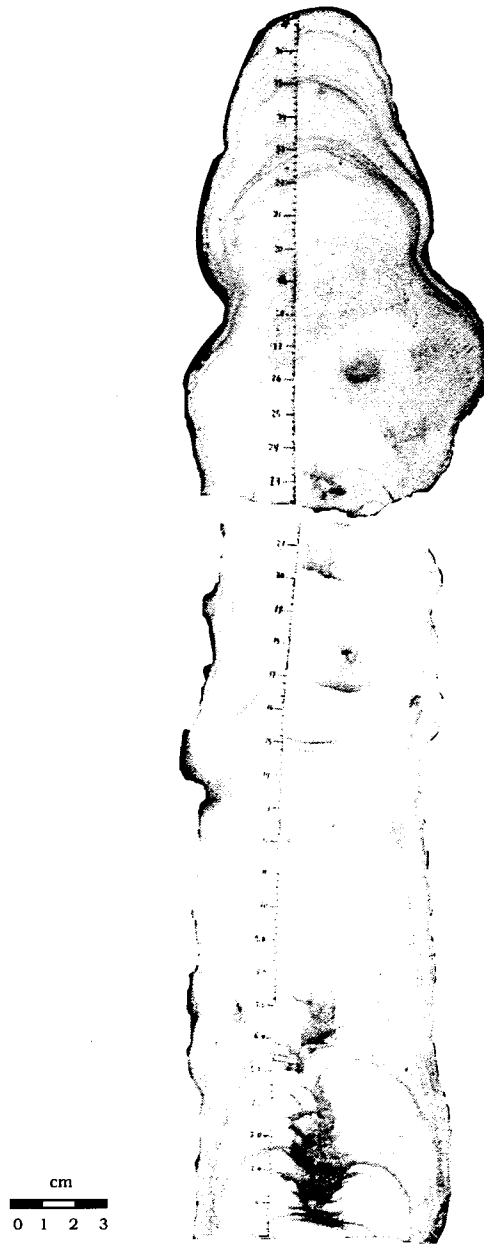
Figure 3.1. Photograph of stalagmite sample CT-7. Major tick marks on sample are in centimeters.

31

PROFILES

PLAN VIEW

TERCIOPELO

Guanacasta Province
Costa Rica
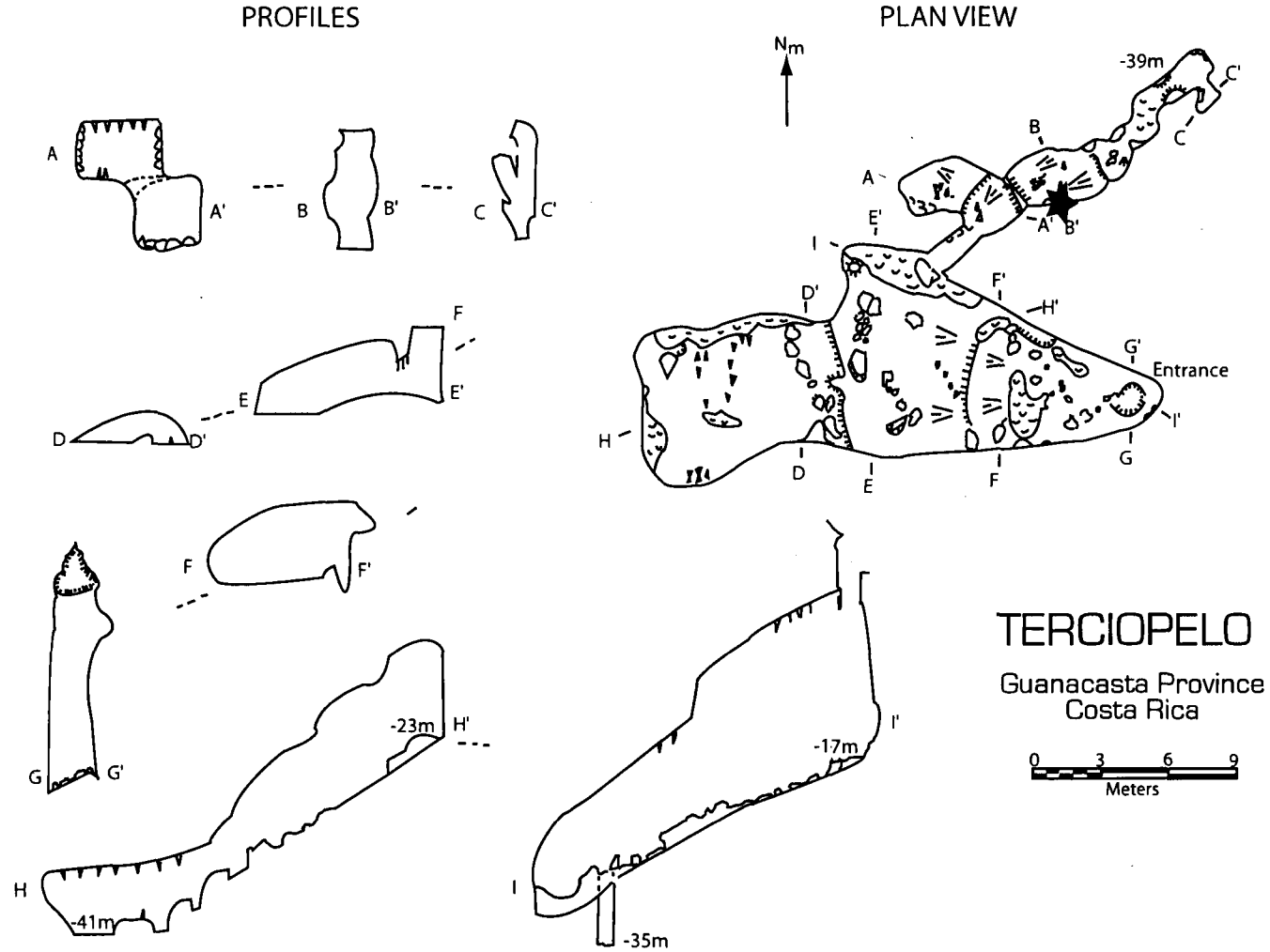
Figure 3.2. Schematic diagram of cave Terciopelo in plan view and in cross-section. Red star indicates sample CT-7 location. Modified from the National Speleological Society Costa Rica Project, 1982.

CHAPTER 4

RESULTS AND INTERPRETATIONS

Cave Environment

The cave from which speleothem sample CT-7 was removed is relatively shallow (≤50 m) below the surface. Rainwater infiltrating through the soil zone and limestone bedrock likely flows into the cave within the same year that it fell. Sample collection occurred in March 2005 during the dry season in northern Costa Rica. Active dripping was occurring very slowly during the dry season in March 2005, suggesting that rainfall during the wet season enters the cave system before the end of the dry season. Since groundwater typically represents the average isotopic composition of rainfall (Darling, 2004), this short residence time allows the climatic $\delta^{18}O$ variability to be recorded in the stalagmite calcite.

Thin Section Qualitative Analysis

Speleothem sample CT-7 contains columnar calcite crystals with irregular and interlocking crystal boundaries. Secondary alteration, such as corrosional features were not found. Laminations are present

33

throughout CT-7, but vary in thickness and continuity. White, relatively porous laminae alternate with slightly darker, more dense laminae throughout the sample. Detrital material, such as silt particles, was not observed in thin section, indicating very clean calcite. Under magnification with cross-polarized light, crystal growth transects laminae throughout the entire length of the sample, suggesting continuous growth with no apparent hiatuses.

Geochronology

The U/Th chemical analyses of four, three- and five-point isochrons produced weighted average dates of 8017± 330 yrs B.P. near the base, and a date of 6639± 250 yrs B.P. near the tip (Table 1). All dates are in correct stratigraphic order, which suggests continuous growth throughout. The final weighted ages were calculated using an Excel add-in ISOPLOT (Ludwig, 2003) and the associated errors are 8017 ± 330 for ISO-1, 7274 ± 290 for ISO-2, 6929± 310 for ISO-3, and 6639 ± 250 for ISO-4. Ages were assigned to stable isotope subsamples according to a linear best fit age model (Figure 4.1) between ~7890 to 6490 yrs B.P using the equation:

Age = -3.79234 × (distance from base in mm) + 7898.32

The isochron methodology was attempted to determine and correct for initial ^{230}Th contamination. Initial $^{230}Th/^{232}Th$ ratios were determined for each isochron: ISO-1, $1.18 \times 10^{-6} \pm 9.7 \times 10^{-5}$ (near base); ISO-2, $1.04 \times 10^{-5} \pm$

34

1.1×10^{-5}; ISO-3, -1.42×10^{-5}± 2.9×10^{-5}; and ISO-4, -3.71×10^{-6} ± 5.7×10^{-6} (near tip). Due to the low ^{230}Th concentration and relatively clean samples with low detritus in thin sections and U-series leachates, the isochron method proved unsuccessful. Although there are four or five subsamples within each isochron, the errors associated with the ^{230}Th/^{232}Th and ^{234}Th/^{232}Th ratios for each subsample are too large to constrain the initial value with precision. Due to the very clean calcite, the ^{230}Th/^{232}Th and ^{230}Th/^{234}Th ratios for each subsample did not provide enough spread in the data. "Dirtier" calcite with more ^{232}Th and/or older samples with more ^{230}Th would have provided a larger spread within the data, which would constrain the initial ^{230}Th/^{232}Th ratios better. The negative initial ^{230}Th/^{232}Th ratios for ISO-3 and ISO-4 are implausible; therefore, by omitting the negative ^{230}Th/^{232}Th ratios, the average ^{230}Th/^{232}Th initial value of ISO-1 and ISO-2 is 5.79×10^{-6}.

Despite a wide range of initial ^{230}Th/^{232}Th values for all four CT-7 isochrons, the "global" initial value of 4.4×10^{-6} was used to correct their ages for detrital thorium, as it falls within the errors of ISO-1 and ISO-2. A global value for initial ^{230}Th/^{232}Th is the best choice, despite the failed attempts of the isochron method. A sensitivity analysis was performed using a ^{230}Th/^{232}Th value of 1.0×10^{-5}, to determine the effect of using a higher value. Although the age model is significantly shifted up to 700 years in some places, in absence of data to the contrary, we use the global initial value. Given continuous growth, CT-7 grew at an average

35

rate of 0.26 mm per year, over ~1400 yrs between the interval 7890 and 6490 yrs B.P.

Stable Isotopes

CT-7 was sampled for stable isotopes at 1mm intervals, therefore representing ~3.79 years of growth between each sample. Stable isotope analysis of CT-7 calcite yielded 372 $\delta^{18}O$ values, excluding 2 outliers, ranging from -11.8‰ to -6.4‰ relative to VPDB. The $\delta^{18}O$ values show a small linear trend, and oscillate about a mean of ~ -8.5‰ (Figure 4.2). Greatest variability occurs between 7200 and 6800 yrs B.P. with a high $\delta^{18}O$ anomaly at ~7000 yrs B.P. In general, the $\delta^{18}O$ values rise slightly from -8.5‰ at ~7890 yrs B.P. to -7.3 at ~7540 yrs B.P., then decline to -9.1‰ at ~7340 yrs B.P. The $\delta^{18}O$ values then rise sharply to -7.4‰ at ~7170 yrs B.P. and then steeply decline to -9.0‰ at ~7120 yrs B.P. The $\delta^{18}O$ values rise again to the most significant peak of -6.7‰ at ~7050 yrs B.P., quickly decline to -8.9‰ at ~6920 yrs B.P., slightly rise to -7.4% at ~6850 yrs B.P., significantly decline to -9.8‰ at ~6610 yrs B.P. and rise to -7.2‰ at ~6490 yrs B.P. at the end of the time series.

Since tropical rainfall $\delta^{18}O$ values are dominated by the amount effect (Dansgaard, 1964), I interpret the $\delta^{18}O$ values in stalagmite CT-7 as a paleo-rainfall record, with higher $\delta^{18}O$ values indicating drier conditions and lower $\delta^{18}O$ values as wetter conditions. The most significant peak

36

occurs at ~7000 yrs B.P., which is interpreted as the most prominent dry period of the record.

The $\delta^{13}C$ time series from stalagmite CT-7 shows values ranging from -11.9‰ to -6.8‰ relative to VBDP (Figure 4.3). There is a large $\delta^{13}C$ decrease of ~5‰ occurring at ~7000 yrs B.P. The $\delta^{13}C$ time series shows much more variability than the $\delta^{18}O$ time series. In general, the $\delta^{13}C$ values increase gradually from -11.2‰ at ~7880 yrs B.P. to -6.9‰ at 7000 yrs B.P., with many oscillations from higher to lower $\delta^{13}C$ values occurring throughout this time period. After the most significant peak at 7000 yrs B.P., there is a dramatic decrease in $\delta^{13}C$ values to -11.6‰ at ~6940 yrs B.P. The $\delta^{13}C$ values then increase gradually to -7.3‰ at ~6680 yrs B.P., decrease rapidly to -11.7‰ at ~6610 yrs B.P. and rise again to -6.8‰ at ~6490 yrs B.P.

Although the $\delta^{13}C$ variations are commonly interpreted to be indicators of vegetation type overlying the cave (Dorale et al., 1998), I interpret the $\delta^{13}C$ variations in stalagmite CT-7 are due to changes in the amount of soil moisture available for biological respiration. All the $\delta^{13}C$ values are within the range of C_3 type vegetation suggesting dry tropical forest was likely present over the cave during the early to mid-Holocene. The variability in the $\delta^{13}C$ time series may be interpreted due to soil moisture variability. The $\delta^{13}C$ record (figure 4.3) shows a broad increasing trend with a maximum $\delta^{13}C$ value ~7000 yrs B.P., which may reflect a general drying trend resulting in a decrease in soil moisture

37

available for biological respiration. At ~7000 yrs B.P., there is a dramatic peak in the $\delta^{13}C$ values, which may reflect a decrease in biological respiration and a decrease in the production of soil biogenic CO_2, resulting from isotopically heavier $\delta^{13}C$ values. I assumed no prior precipitation of calcite, which would produce an increase in the $\delta^{13}C$ values. Therefore in order to produce a decrease in biological respiration, a shift in climate to drier conditions must occur. Drier conditions would produce less water infiltrating into the soil zone and limit biological respiration which decreases soil pCO_2. Higher $\delta^{13}C$ values therefore result from less biological respiration within the soil zone, and a decrease in the proportion of soil CO_2 to the contributing drip waters, which should produce a $\delta^{18}O$-$\delta^{13}C$ correlation.

Grayscale Analysis

Grayscale analysis yielded 19,651 grayscale values ranging from 105 to 227, with a value of 0 representing white, and a value of 255 representing black. With the use of the NIH grayscale program SCION, very high resolution sampling was possible at less than 1 year resolution. The grayscale values show a gradual decrease from 227 at ~7900 yrs B.P. to 110 at ~7230 yrs B.P (Figure 4.4). There is a sharp increase in values to 198 at 7060 yrs B.P., which represents one of the most significant peaks in the time series. There is a sharp decline to a

38

grayscale value of 109 at ~6920 yrs B.P. and then a gradual increase in values until 218 at ~6480 yrs B.P

Speleothems commonly contain annual couplets of white porous calcite, and dark compact calcite, resulting from seasonal variations in supersaturation and rate of dripwaters (Genty and Quinif, 1996; Genty et al., 1997). Although sample CT-7 does not appear to contain annual banding in which to observe seasonal fluctuations, I interpret the dark dense bands represent dry conditions, while the white porous bands are indicative of increased precipitation events (Figure 4.4). During periods of increased precipitation, more water is able to infiltrate through the soil zone, resulting in faster drip rate into the cave system, producing faster growing speleothems with lighter and more porous bands. During dry conditions, less infiltration occurs, producing slower drip rates into the cave leading to darker and denser bands.

Fourier Analyses

Spectral analysis based on the Lomb-Scargle Fourier transform, which uses a program (REDFIT) (Schulz and Mudelsee, 2002), allowed for direct processing of an unevenly spaced time series without the requirement of interpolation between data points. Analysis on the oxygen isotope time series suggests statistically significant variance at the 99% confidence interval to occur at 191 years (Figure 4.5). At the 95% confidence interval, statistically significance variance is occurring at 15,

39

12, and 10 years. At the 90% confidence interval, statistically significant variance is occurring at 15 and 13 years. At the 85% confidence interval, statistically significant variance is occurring at 25, 20, and 8 years.

The Lomb-Scargle Fourier transform method on the carbon isotope time series suggests no statistically significant variance occurring at the 99% confidence interval. At the 95% confidence interval, there is statistical power occurring at 25 and 16 years (Figure 4.6). At the 90% confidence interval, statistically significant variance is occurring at 11 years. At the 85% confidence interval, statistical power is occurring at 14, 9, and 8 years.

Analysis on the grayscale time series suggests statistically significant variance at the 99% confidence interval occurring at 13, 12, 5, 4, 3, and 2 years (Figure 4.7). At the 95% confidence interval, statistical power is occurring at 19, 5 and 3 years. At the 90% confidence interval, there is statistical power at 9 and 6 years. At the 85% confidence interval, statistically significance variance occurring at 15 and 7 years, with many peaks of statistical power ranging from 6-2 years.

Another form of spectral analyses, called wavelet analysis, was also performed on the time series. Oxygen isotope time series at the 2-8 year time scale suggest statistically significant variance occurring at ~6800 and ~7500 years B.P (Figure 4.8). On the 10-20 year time scale, statistically significant variance is occurring at ~6800 years B.P. No

40

statistically significant variance at the 95% confidence interval was present at the 20-30, 30-50, 50-70, or 70-100 time periods.

Wavelet analysis was also performed on the carbon isotope time series and suggests statistically significant variance occurring at the 10-20 year time scale at ~6500, 6700, 6800, 7200, and 7300 years B.P (Figure 4.9). At the 20-30 year time scale, statistically significant variance is occurring at ~6700 years B.P. On the 30-50 year time scale, significant variance is occurring at ~6600 years B.P. There is no significant variance occurring on the 2-8, 30-50, 50-70, and 70-100 time scales.

Wavelet analysis suggests that the grayscale time series produces statistically significant variance throughout the growth period of stalagmite CT-7 at all time periods (2-8, 10-20, 20-30, 30-50, 50-70, and 70-100) (Figure 4.10).

42

Sample ID	distance from base (mm)	U(ppm)	±2σ	Th(ppm)	±2σ	^{230}Th/^{232}Th$_{ppm}$	±2σ	^{230}Th/^{238}U (Activity)	±2σ	δ^{234}U$_i$	±2σ	Corrected Age (B.P.)	±2σ
CT-7 1A	11	0.09	5.06E-04	5.03E-04	1.27E-05	206.70	5.36	6.03E-03	0.0002	-6.49	11.27	8223	658
CT-7 1B	11	0.06	3.13E-04	4.00E-04	1.22E-05	183.39	5.66	6.56E-03	0.0002	-11.47	7.14	7949	459
CT-7 1C	11	0.08	4.58E-04	3.80E-04	1.65E-05	235.29	10.31	5.20E-03	0.0002	11.94	8.52	7945	676
ISO-1 (weighted average)												8019	340
CT-7 2A	110	0.08	3.74E-04	1.56E-03	1.45E-05	59.05	0.62	2.05E-02	0.0002	22.27	8.64	7347	598
CT-7 2B	110	0.06	2.87E-04	8.76E-04	2.04E-05	84.23	1.99	1.40E-02	0.0003	-1.64	11.96	7479	728
CT-7 2C	110	0.09	2.96E-04	8.55E-04	1.40E-05	108.57	1.82	1.03E-02	0.0002	8.56	6.96	7098	504
CT-7 2D	110	0.08	2.87E-04	1.43E-03	1.85E-05	64.13	0.86	1.92E-02	0.0003	-0.65	7.97	7699	609
CT-7 2E	110	0.09	2.71E-04	1.91E-03	1.52E-05	43.48	0.37	2.23E-02	0.0002	-2.59	3.63	5826	1178
ISO-2 (weighted average)												7244	340
CT-7 3A	245	0.09	4.22E-04	5.53E-04	1.37E-05	172.42	4.36	6.57E-03	0.0002	8.74	7.55	7313	552
CT-7 3B	245	0.08	3.66E-04	9.02E-04	1.15E-05	98.81	1.33	1.11E-02	0.0001	39.18	8.53	6693	599
CT-7 3C	245	0.08	6.66E-04	6.20E-04	1.78E-05	136.43	4.07	7.68E-03	0.0002	-3.47	16.77	6783	493
ISO-3 (weighted average)												6939	330
CT-7 4A	355	0.08	3.39E-04	1.26E-03	1.16E-05	68.20	0.69	1.58E-02	0.0002	-0.98	7.31	6755	500
CT-7 4B	355	0.09	3.13E-04	2.12E-03	1.27E-05	42.29	0.30	2.50E-02	0.0002	6.78	5.70	6287	421
CT-7 4C	355	0.09	2.96E-04	1.41E-03	1.07E-05	69.54	0.58	1.66E-02	0.0001	2.90	5.61	7226	609
CT-7 4D	355	0.09	5.36E-04	1.12E-03	2.11E-05	79.71	1.58	1.33E-02	0.0003	-4.85	8.61	6703	754
CT-7 4E	355	0.09	5.59E-04	1.14E-03	1.22E-05	74.89	0.94	1.38E-02	0.0002	-0.78	14.68	6512	853
ISO-4 (weighted average)												6717	340

Table 1. Uranium/ thorium radiometric isotopic data and ages for sample CT-7. Isochrons are abbreviated as ISO and represent the weighted average of 3-5 subsamples along the same growth layer.
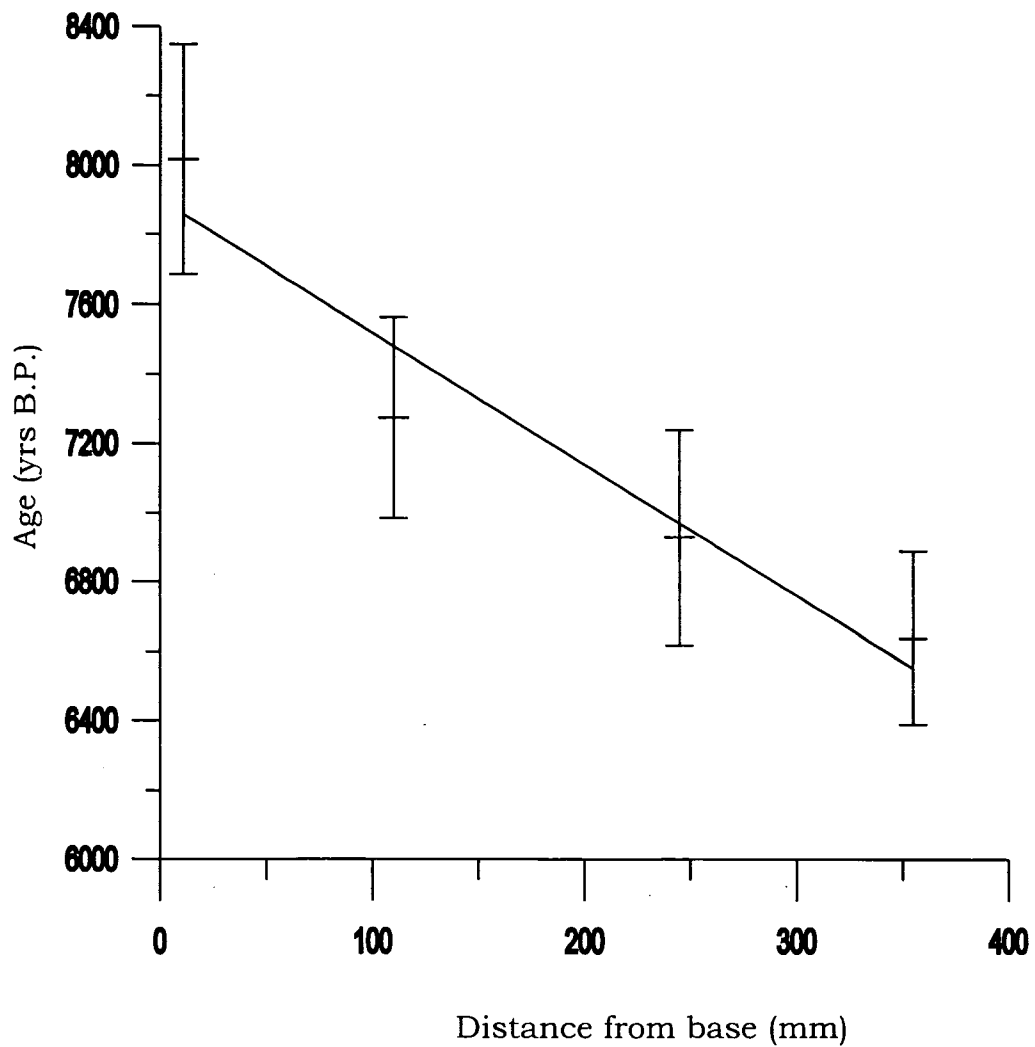
Figure 4.1. Chronology of CT-7 versus distance from the base in mm. Ages are based on U/Th dating. Each data point represent the weighted average of 3-5 subsamples along the same growth layer. The associated errors with each data point is represented by error bars. A linear trendline was fit to the data.

43
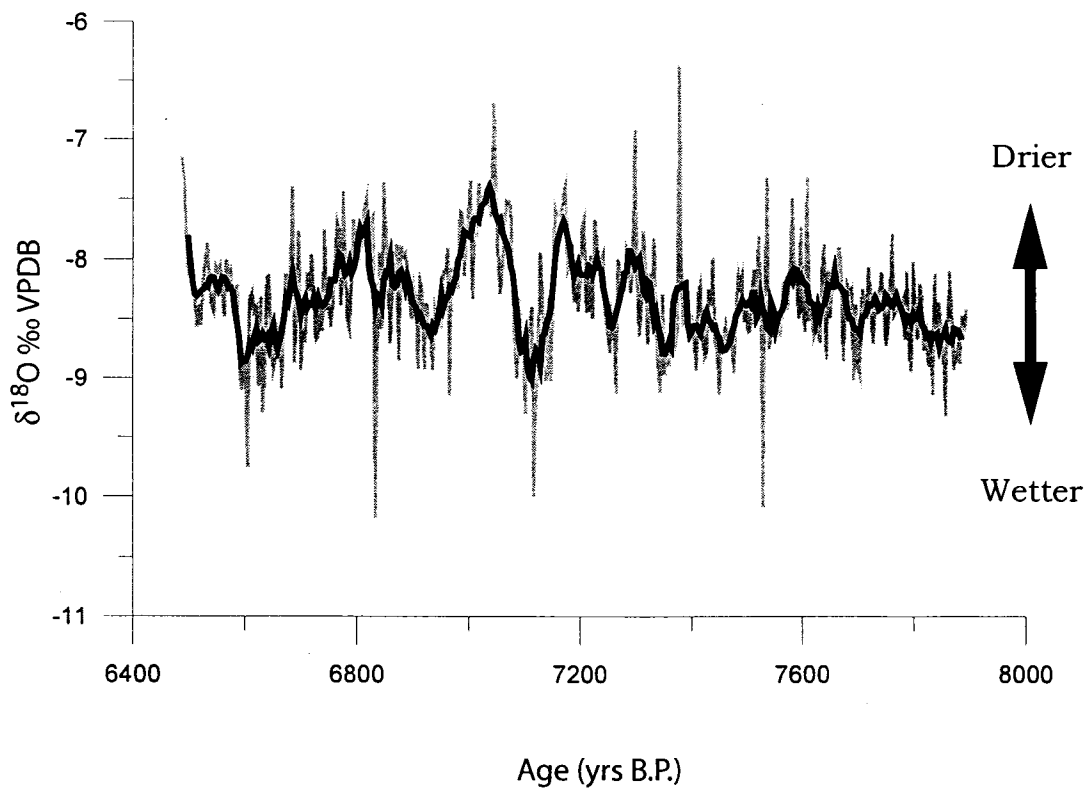
Figure 4.2. $\delta^{18}O$ time series with values ranging from ~-6.5 to -10‰. The gray line represents the raw data and the bold black line represents the 7-pt running average. A significant peak occurs at ~7000 years B.P. Values vary about a consistent mean of ~-8.5‰.

44
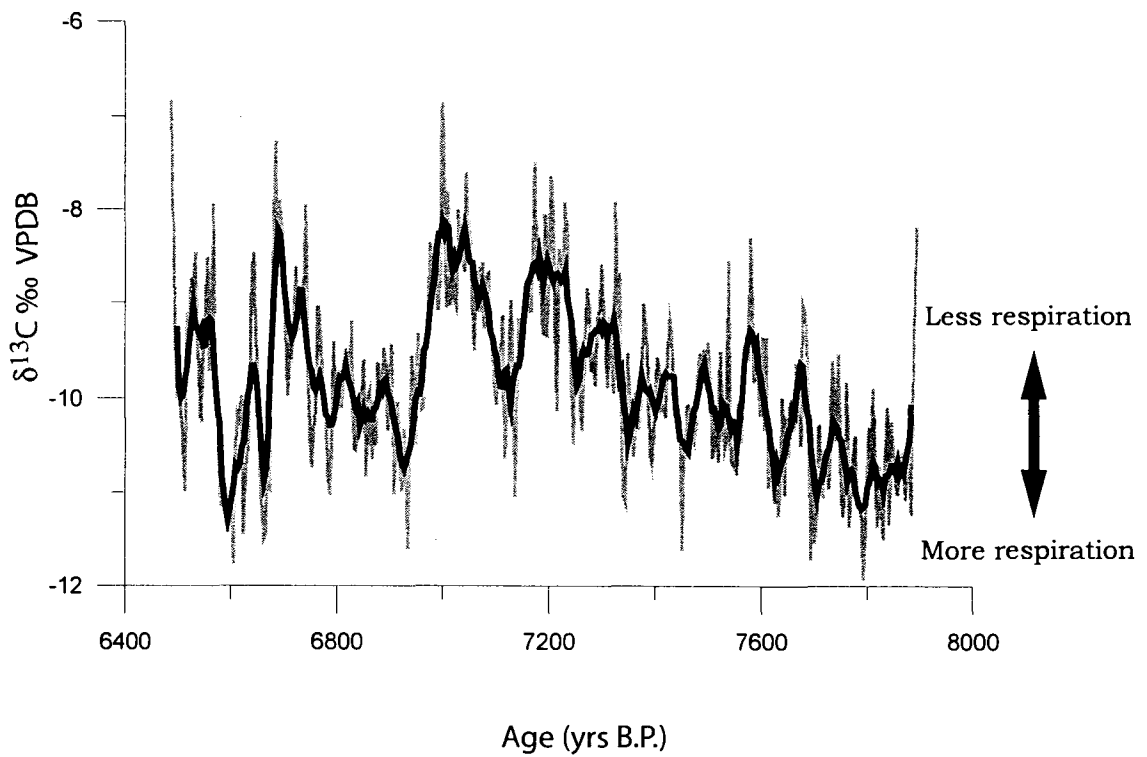
Figure 4.3. $\delta^{13}C$ time series with values ranging from ~-7 to -12‰ with the most significant peak occuring at ~7000 years B.P. The gray line represents the raw data and the bold black line represents the 7-pt running average.

45
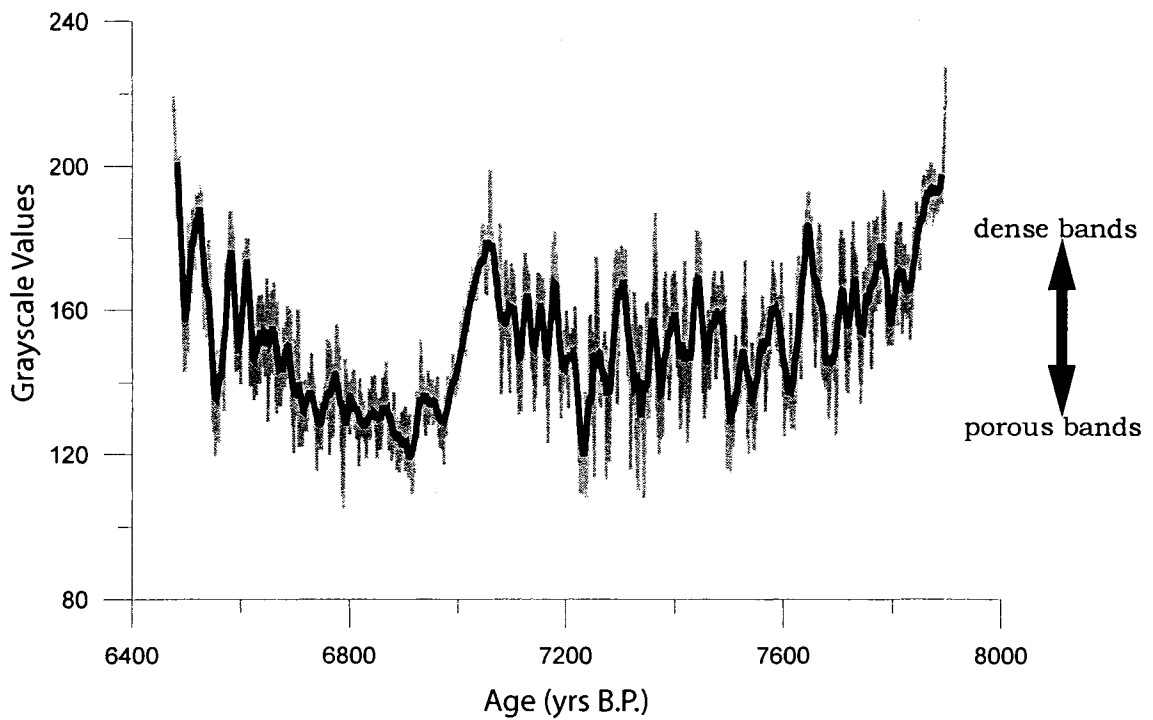
Figure 4.4. Grayscale time series with values ranging from ~100-220. The gray line represents the raw data and the bold black line represents the 215-pt running average. Grayscale values are a result of digital image processing, in which sample CT-7 was illuminated with UV light and then converted into a grayscale record. A value of zero represents white and a value of 255 represents black.

46

δ¹⁸O Spectral Analysis
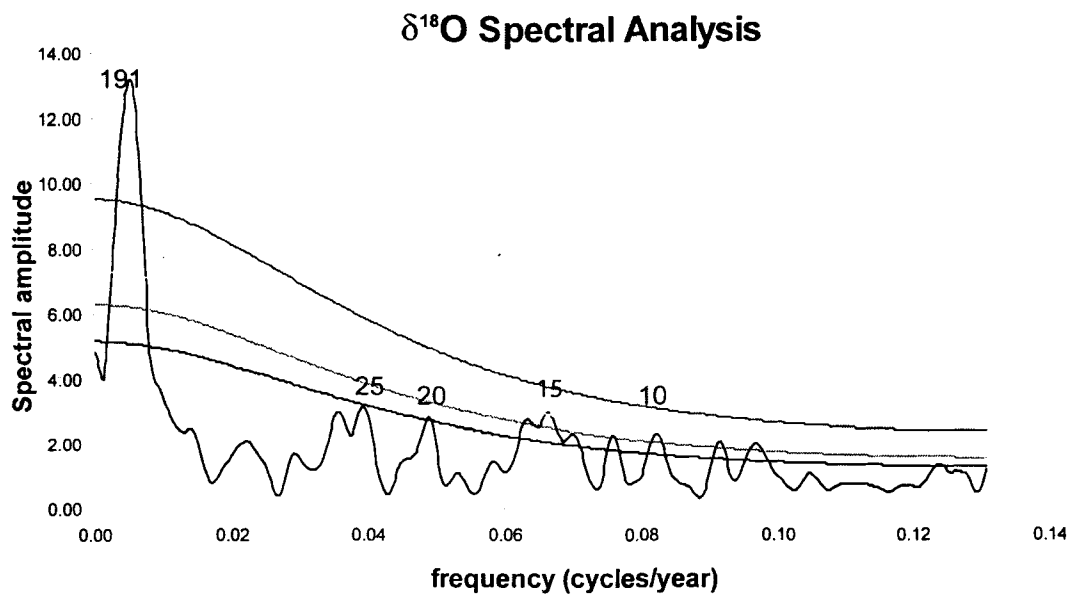
Figure 4.5. Spectral analysis of the $\delta^{18}O$ time series illustrating the 99, 95, 90, and 85% confidence intervals (from top to bottom). The numbers above the peaks represent the years of statistical significance.

47
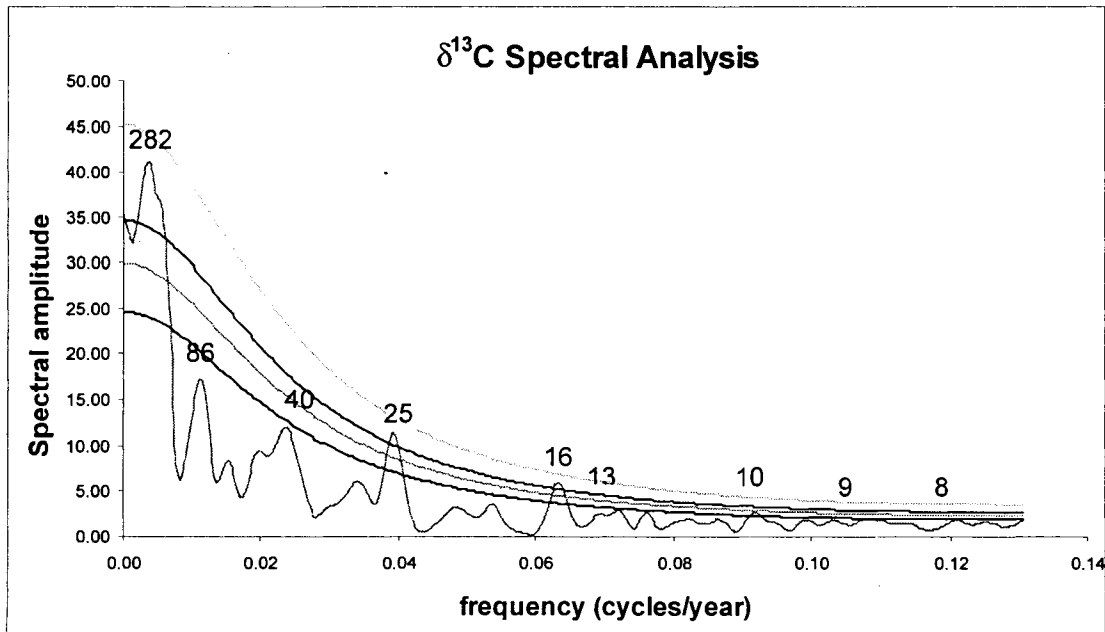
Figure 4.6. Spectral analysis of the $\delta^{13}C$ series illustrating the 99, 95, 90, and 85% confidence intervals (from top to bottom). The numbers above the peaks represent the years of statistical significance.
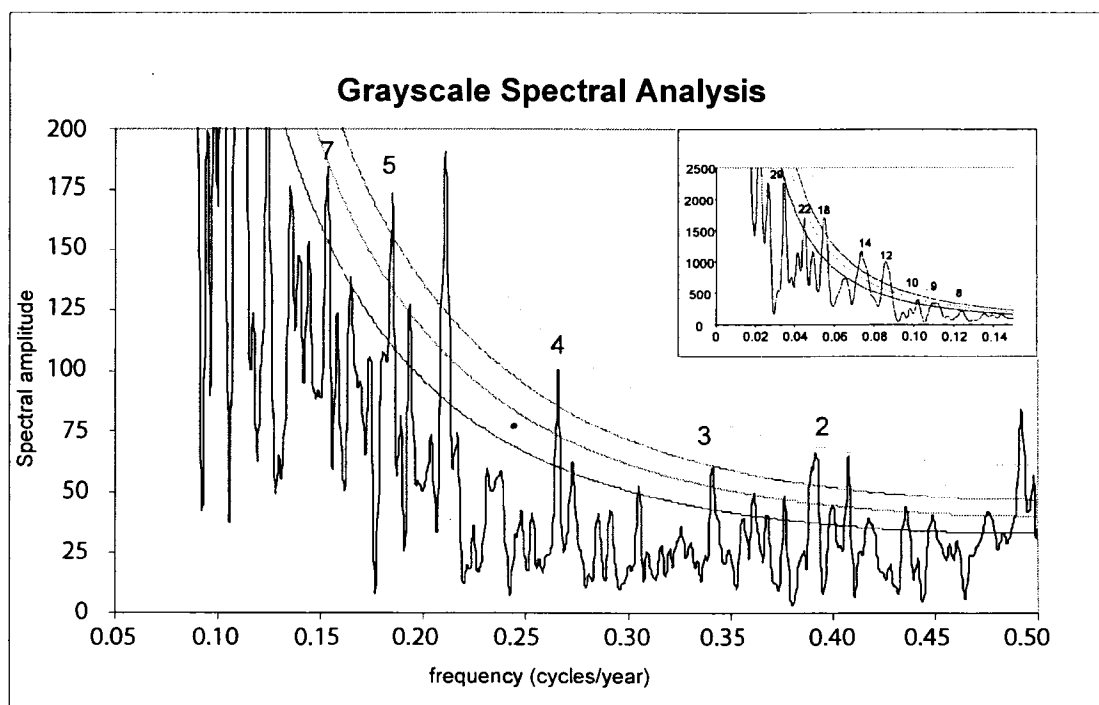
Figure 4.7. Spectral analysis of the grayscale time series illustrating the 99, 95, 90, and 85% confidence intervals (from top to bottom). The numbers above the peaks represent the years of statistical significance.

49

A.

CT-7 $\delta^{18}O$ values between 6490 and 7890

B.

CT-7 $\delta^{18}O$ Wavelet Power Spectrum
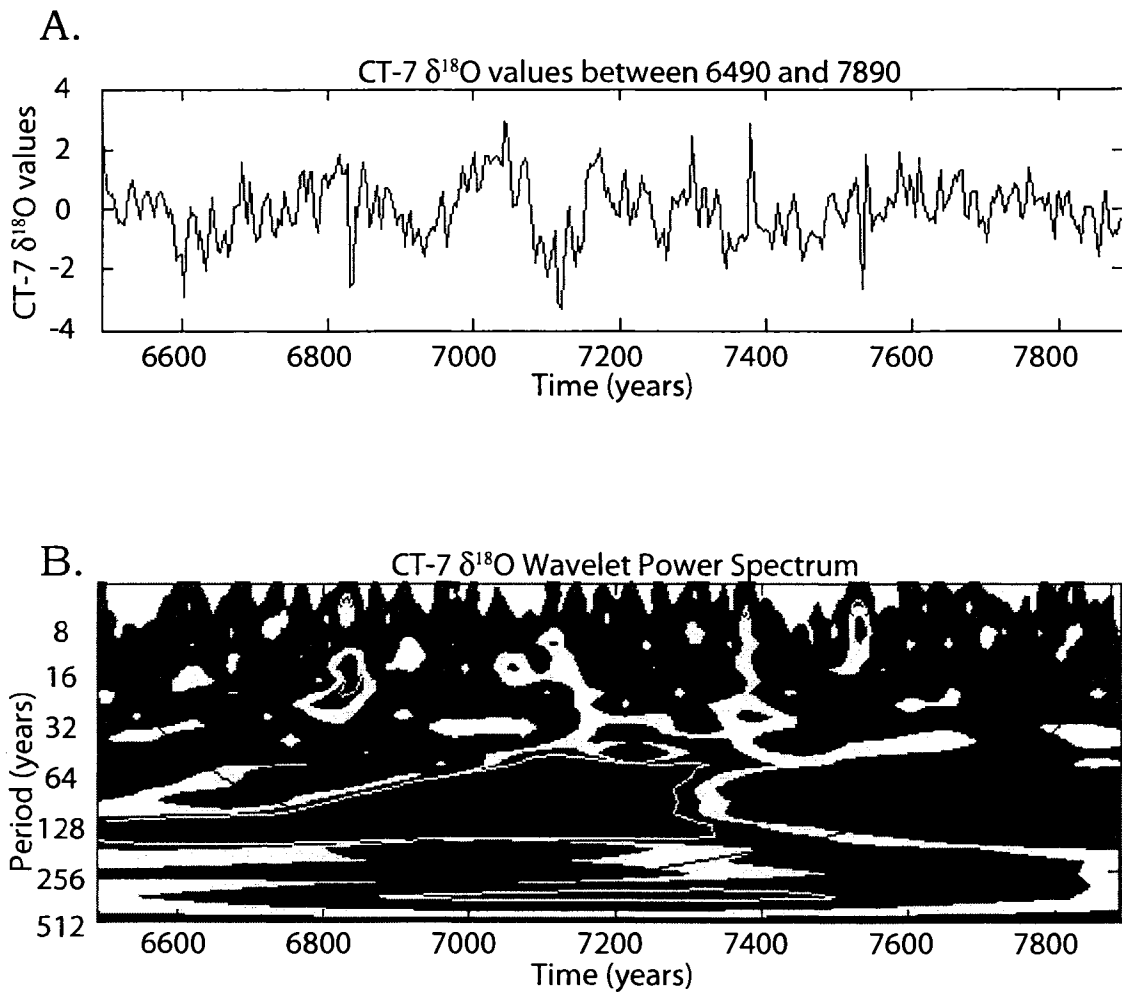
Figure 4.8. Wavelet analysis on $\delta^{18}O$ time series. A) Detrended normalized data in standard deviation units. B) Wavelet power spectrum for 3.8 year sampled $\delta^{18}O$ values. White contours represent 95% confidence interval.

50

A.

CT-7 δ^{13}C values between 6490 and 7890

B.

CT-7 δ^{13}C Wavelet Power Spectrum
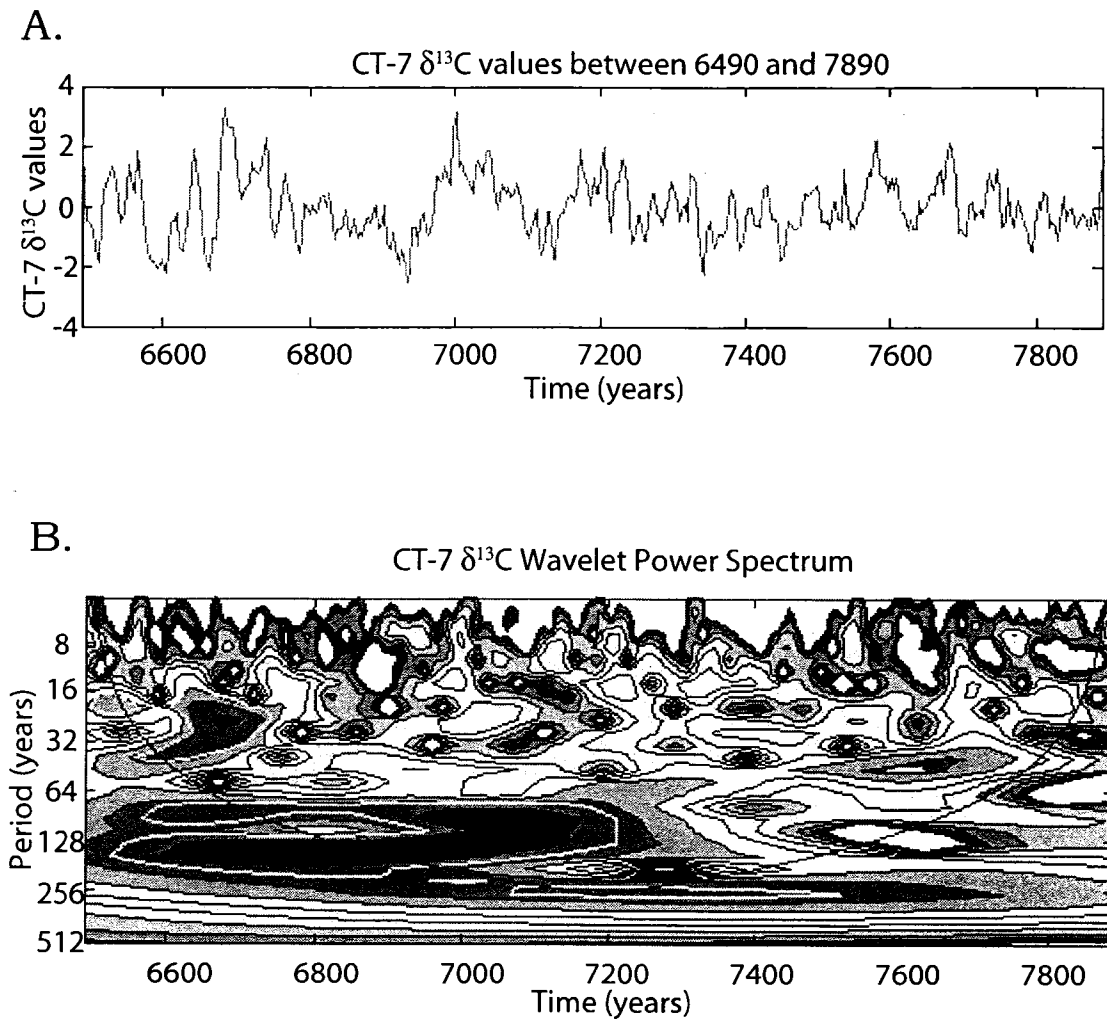
Figure 4.9. Wavelet analysis on δ^{13}C time series. A) Detrended normalized data in standard deviation units. B) Wavelet power spectrum for 3.8 year sampled δ^{13}C values. White contours indicate the 95% confidence interval.

51

A.

CT-7 Grayscale values between 6490 and 7890 yrs B.P.

B.

CT-7 Grayscale Wavelet Power Spectrum

C.

2-8 yr Scale average Time Series
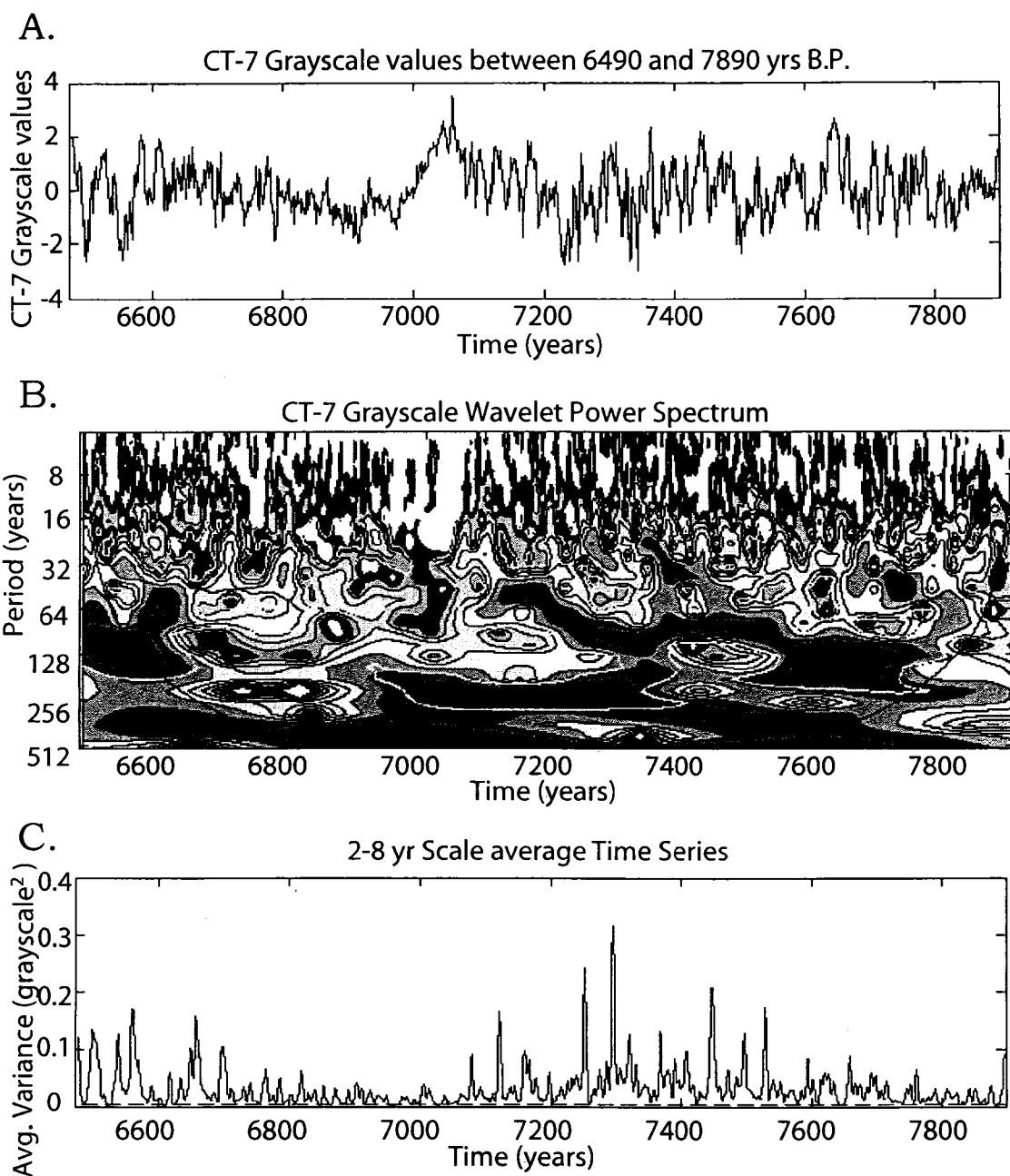
Figure 4.10. Wavelet analysis on grayscale time series. A) Detrended normalized data in standard deviation units. B) Wavelet power spectrum for 1 year sampled grayscale values. White contours indicate the 95% confidence interval. C) 2-8 yr scale average time series. Dotted line represents the 95% confidence interval. Data above the dashed line indicates statistically significant variance.

52

CHAPTER 5

DISCUSSION

ENSO and the PDO

The $\delta^{18}O$ values obtained from CT-7 are interpreted as a rainfall proxy

and are used to evaluate if El Niño became more active since ~7ka

(Rodbell et al., 1999; Moy et al., 2002; Sandweiss et al., 2001). The $\delta^{18}O$

values show rainfall varied about a consistent mean with no large

isotopic shifts in $\delta^{18}O$ values (Figure 5.1 A). This suggests there was no

significant rainfall regime shift throughout the growth of stalagmite CT-7.

A climatic regime shift is defined as a transition from one climatic state

to another, within a period substantially shorter than the lengths of each

climatic state (Minobe, 1997). A major regime shift would have a

noticeable shift in the $\delta^{18}O$ values and/or a shift in variability, from low

to high frequency variability (or vice versa), after 7000 yrs B.P., but no

such shift is evident.

To evaluate the relationship between rainfall $\delta^{18}O$ values and ENSO

events, the $\delta^{18}O$ time series was compared with an El Niño proxy record

spanning 15 ka from Laguna Pallcacocha, Ecuador (Figure 5.1 D)

(Rodbell et al., 1999; Moy et al., 2002). In the Laguna Pallacocha record,

53

the deposition of clastic laminae were suggested to be a direct response to slope erosion associated with heavy El Niño rainfall events (Rodbell et al., 1999). The Pacific coast of South America experiences anomalous wet conditions during El Niño years due to the southern position of the ITCZ. After 7000 yrs B.P., the Laguna Pallcacocha record shows an increase in clastic laminae deposits, and an increase in ENSO-band variance, but the CT-7 $\delta^{18}O$ values do not show an increase in $\delta^{18}O$ variability after 7000 yrs B.P. A possible explanation for the lack of correlation between the two records could be that the wet season may have become shorter due to the southward migration of the ITCZ, but the intensity of rainfall and thus the $\delta^{18}O$ values remained the same. Although I observe a $\delta^{18}O$ peak at 7 ka, representing the most intense dry period, there is no evidence for enhanced $\delta^{18}O$ variability after this time, as would be expected if El Niño became more dominant. Spectral analysis of the CT-7 $\delta^{18}O$ values display decadal to multidecadal variability, indicating that low frequency ENSO-band variance was present throughout the middle Holocene.

Many researchers suggested that modern ENSO events began between 7000 and 5000 yrs B.P. and have increase in frequency and intensity to the present (Sandweiss et al., 2001; Rodbell et al., 1999; Moy et al., 2002). Sandweiss et al. (2001) suggested that modern ENSO events were absent before 5800 yrs B.P. in Peru, but spectral analysis of CT-7 grayscale values indicate decadal to multidecadal climate variability

54

throughout the mid-Holocene. Speleothem luminescence, which I
interpret as a rainfall/moisture proxy record, displays dark dense bands
representing slow drip rates and drier conditions, and white porous
bands indicative of increased drip rates and wetter conditions. An
important feature of the normalized/detrended grayscale time series
(Figure 4.10 A) is a change in character of variability at ~7ka. Although
previous studies suggested an increase in ENSO-band variance after 7ka
(Koutavas et al., 2002; Otto-Bleisner, 1999; Tudhope et al., 2001;
Clement et al., 2000), CT-7 grayscale analysis indicates greater
variability before this time. Despite the evidence from South America
suggesting that ENSO was weak or absent prior to ~5800 yrs B.P.
(Sandweiss et al., 2001), the CT-7 grayscale time series suggest that
ENSO-band variance was occurring throughout the mid-Holocene.

The coupled interactions of the ocean-atmosphere system associated
with ENSO occur on both annual and seasonal cycles, and are also
affected by extra-tropical forcings (Clement et al., 1999). Evidence of an
active PDO during the middle Holocene is suggested by spectral analysis
of the $\delta^{18}O$ time series, which illustrates spectral power occurring at
decadal to multi-decadal periodicities (Figure 4.5). Minobe (1999, 2000)
used wavelet analysis of SST and SLP from the North Pacific (north of 20°
N), the epicenter of the PDO, and found the most statistical power
occurring in the 15-25 year and 50-70 year periodicities. The PDO
produces similar climate anomalies as those produced with ENSO

55

variations, though not as extreme (Mantua and Hare, 2002). In Central America and northern South America, the warm phase of the PDO coincide with dry periods, much like the warm phase of ENSO (Mantua and Hare, 2002). Although there are many dendroclimatic reconstructions of the PDO (e.g. Arrigo et al., 2001; Biondi et al., 2001; Gray et al., 2003), the CT-7 $\delta^{18}O$ time series indicates rainfall variability on decadal to multidecadal timescale, suggesting that the PDO was active at modern periodicities during the middle Holocene. Decadal to centennial scale climate variability is present in the $\delta^{18}O$ record of forams from a Santa Barbara Basin sediment core, and provides supporting evidence from modern PDO periodicities during the mid-Holocene (Friddell et al., 2003).

The main evidence for an active PDO during the middle Holocene is suggested by wavelet analysis of the grayscale time series, which illustrates statistically significant variance occurring at the two main PDO periodicities, 15-25 and 50-70 years (Minobe, 1997), throughout the interval of growth. Despite the lack of PDO periodicities in the $\delta^{18}O$ and $\delta^{13}C$ wavelet analysis, the presence of PDO-band variance in the grayscale time series is interpreted as indicating that the PDO was active throughout the middle Holocene.

Solar Variability

Variations in solar activity and intensity are recorded by $\Delta^{14}C$ variations (Stuiver and Braziunas, 1993) from tree rings and other proxy data, and has been suggested as the primary control on centennial to decadal scale changes in rainfall and intensity of the Indian Ocean monsoon (Neff et al., 2001). Although there is no direct correlation between the atmospheric $\Delta^{14}C$ data and the CT-7 $\delta^{18}O$ values, spectral analysis of the $\delta^{18}O$ time series indicates statistically significant power at 10 and 191 years, which are similar to the 11 and 206 year solar cycles, and may be a result of solar forced variations in atmospheric $\Delta^{14}C$ values. Minor variations in solar variability could be amplified due to changes in atmospheric and/or oceanic circulation (Neff et al., 2001) and therefore, may result in some feedback mechanism that can act together with ENSO producing regional climatic anomalies in Central America.

Atlantic Climate Variability

Although modern climate variability in the Pacific Ocean is dominated by ENSO and the PDO, Costa Rica may also be affected by Atlantic Ocean variability. For example, ENSO forces weaker Atlantic SST anomalies with a lagged response of approximately 8 months (Hastenrath, 1978). Evidence from GCM modeling studies suggests that the Atlantic Ocean is also capable of forcing rainfall anomalies throughout northeast South America. When warm SST anomalies occur

57

in the north tropical Atlantic, northeast South America experiences dry conditions, similarly to Costa Rica. Therefore, climate variability in the Atlantic, such as the North Atlantic Oscillation (NAO) and Atlantic Multidecadal Oscillation (AMO), may also affect climate in Costa Rica.

Carbon Isotopes

Paleoenvironmental interpretations based on speleothem $\delta^{13}C$ values are extremely complex due to the many factors that can influence $\delta^{13}C$ values. Both equilibrium and kinetic fractionation can alter the $\delta^{13}C$ values. Although the raw $\delta^{13}C$ and $\delta^{18}O$ correlation show a weak relationship most likely due to high frequency noise ($r^2=0.36$), the 7-pt running averaged $\delta^{13}C$ and $\delta^{18}O$ values are highly correlative ($r^2=0.68$), suggesting a common forcing mechanism for the covariation. Covariation between the $\delta^{18}O$ and $\delta^{13}C$ values is likely to be due to variations in soil respiration rates. I interpret higher (lower) $\delta^{13}C$ values coincide with drier (wetter) conditions inferred from the $\delta^{18}O$ record, which is a common relationship observed in other tropical stalagmites (Burns et al., 2002). Drier periods may result in a thinner water film on the tip of the stalagmite due to slower drip rates into the cave, enhancing CO_2 degassing and enriching the $\delta^{13}C$ values. In regions where the amount effect is the dominant isotopic control, reduced rainfall increases the $\delta^{18}O$ values which may be enhanced by evaporation within the cave in correlation with $\delta^{13}C$ values (Fleitmann et al., 2004), although

58

evaporation within poorly ventilated tropical cave systems, such as Terciopelo cave, is not likely. It may be possible that the $\delta^{13}C$ values in speleothems are more sensitive indicators of climate variability than $\delta^{18}O$ values in the tropics, as suggested by increased variability in the $\delta^{13}C$ time series (Figure 4.3) compared to the $\delta^{18}O$ time series (Figure 4.2)

Similarly, $\delta^{13}C$ variations have been linked to variations in ENSO strength and frequency, producing variations in tropical rainfall $\delta^{18}O$ values which forces changes in biological respiration rates in the soil zone (Frappier et al., 2002; Burns et al, 2002). $\delta^{13}C$ values from a speleothem in Belize reveal a strong correlation to the Southern Oscillation Index (SOI), providing evidence that ENSO-related changes in the terrestrial carbon cycle can be recorded by speleothems, despite the fact that Belize does not experience a change in weather patterns commonly associated with the SOI (Frappier et al., 2002). The CT-7 $\delta^{13}C$ values indicate that although the climatic response to ENSO may be weak, as suggested by the $\delta^{18}O$ values, the ecological system may be more sensitive to climatic variability (Frappier et al., 2002).

Covariation

Figure 5.2 illustrates that $\delta^{18}O$, $\delta^{13}C$, and grayscale values vary in a consistent manner, which are interpreted as being forced by changes in the amount of precipitation. The presence of common peaks (labeled #1-12) in the $\delta^{18}O$, $\delta^{13}C$, and grayscale time series, imply that there is a

common forcing mechanism responsible for the observed covariation. If all three proxies display similar patterns of change and/or trends, then it is likely that a common environmental variable is involved (Curtis et al., 1998). Rainfall variability is interpreted as the dominant force affecting grayscale values, and therefore, grayscale values can also be used as a moisture proxy. The observed covariation between the $\delta^{18}O$, $\delta^{13}C$, and grayscale values is interpreted as being forced by rainfall, such that during El Niño events and/or the warm phase of the PDO, drier conditions occur on the Pacific slope of Costa Rica (Waylen et al., 1996). Drier conditions (high $\delta^{18}O$ values) lead to a decrease in soil moisture and a decrease in biological respiration (high $\delta^{13}C$ values). As a result of a drier climate, less water percolates through the soil zone and into the cave, resulting in darker/denser laminae (high grayscale values).

60
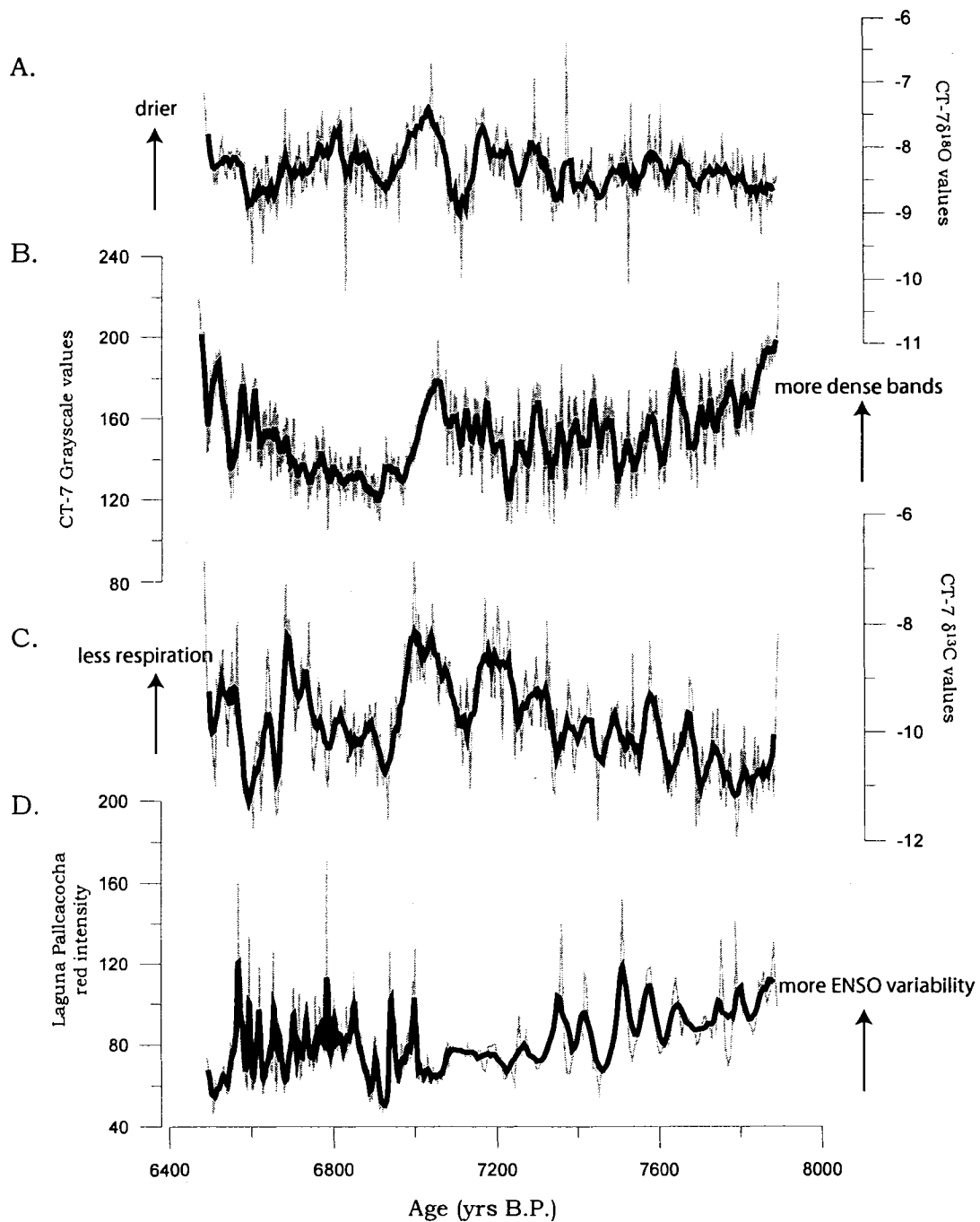
Figure 5.1. Comparison between the Laguna Pallcacocha ENSO red intensity record (Moy et al., 2002) and CT-7. A) CT-7 $\delta^{18}O$ values with 7-pt running average in bold. B) CT-7 grayscale values with 215-pt running average in bold. C) CT-7 $\delta^{13}C$ values with 7-pt running average in bold. D) Laguna Pallcacocha, Ecuador sediment core red intensity record with 7-pt running average in bold.

61
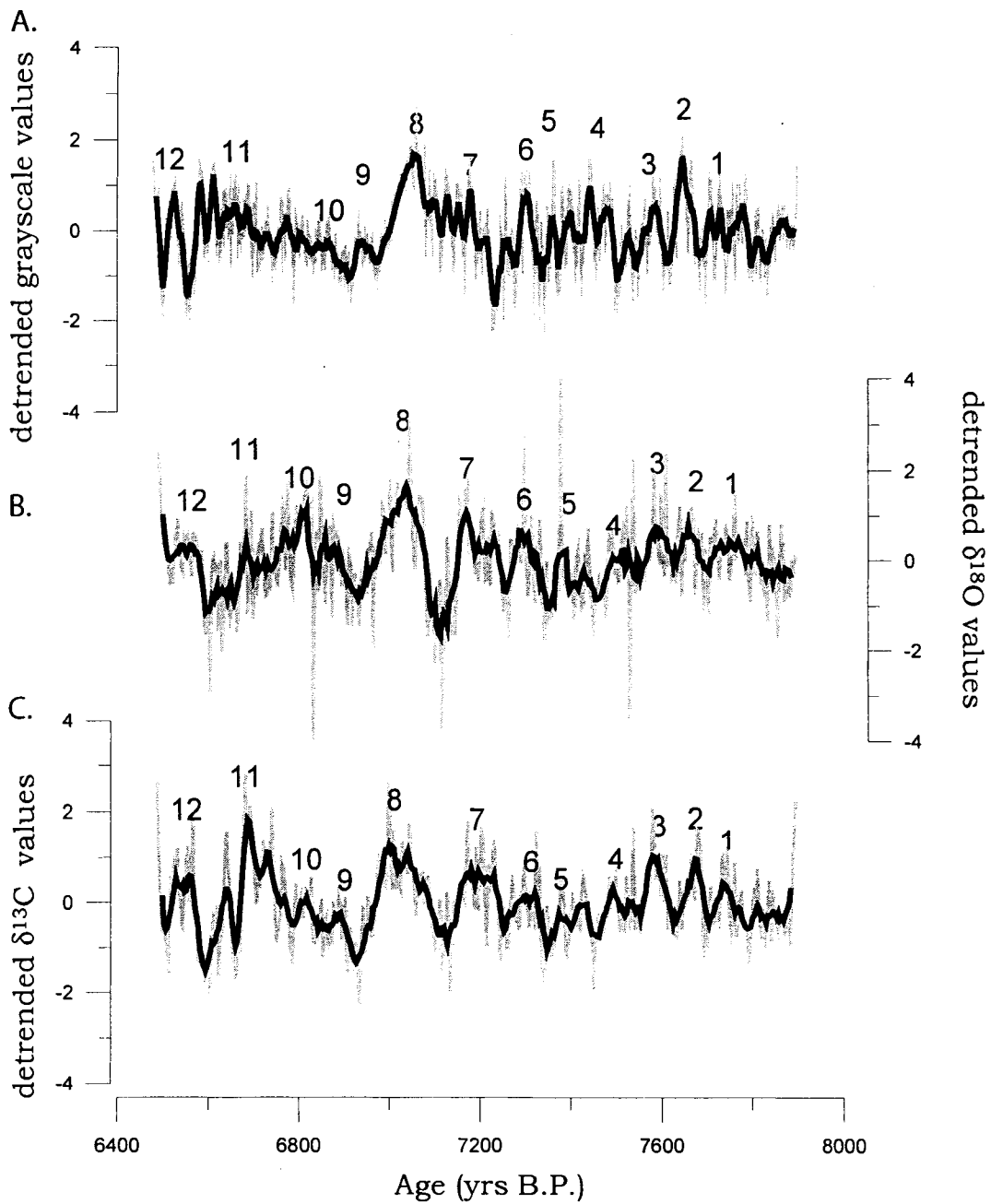
Figure 5.2. Comparisons of all three detrended/normalized data sets with a 7-pt running average superimposed for the $\delta^{18}O$ and $\delta^{13}C$ time series and a 215-pt running average for the grayscale time series, which illustrate correlative peaks labeled by #1-12. A) Grayscale time series. B) $\delta^{18}O$ time series. C) $\delta^{13}C$ time series. Data shown in standard deviation units.

62

CHAPTER 6

CONCLUSIONS

Variations in ENSO and the PDO impact climate worldwide due to

changes in the heat budget of the tropical Pacific, which can disrupt

weather patterns in remote regions due to the complex teleconnections of

the ocean-atmosphere system. The middle Holocene is a key time period

in which many proxy records suggest the onset of modern ENSO

conditions (Sandweiss et al., 2001, Rodbell et al., 1999; Moy et al., 2002).

Speleothems from tropical areas are ideal geologic material that can

be used as terrestrial paleoclimate proxies because they can be precisely

dated using U-series isotopes and may grow continuously for several

thousand years. Speleothem-based ENSO paleoclimate records can

provide high-resolution records that extend the climate record to pre-

historical times and can elucidate Pacific climate variability.

During the mid-Holocene, proxy evidence and modeling studies

suggest a suppressed and/or weakened ENSO compared to the modern

ENSO cycle (Clement et al, 2000; Tudhope et al., 2001; Otto-Bleisner,

1999), but this study suggests that in Costa Rica, and most likely

throughout much of Central America, low-frequency ENSO and the PDO

63

persisted throughout the mid-Holocene, from ~7890 and 6490 yrs B.P. The $\delta^{18}O$ and grayscale values from stalagmite CT-7 suggest there was no significant regime shift at ~ 7 ka, rather persistent decadal to multidecadal variability is occurring throughout the sample. Low-frequency ENSO and/or the PDO seem to be operating in Costa Rica throughout the mid-Holocene.

Despite the complex processes and mechanisms that influence $\delta^{13}C$ values in speleothem calcite, the $\delta^{13}C$ values obtained from stalagmite CT-7 most likely record vegetation type and variations in the amount of biological respiration, If this is the case, the $\delta^{13}C$ values may be a more sensitive climate proxy than $\delta^{18}O$ values in the tropics. Grayscale values are assumed to be dependent on the amount of infiltrating water into the cave system and can provide an additional proxy for infiltration/drip rate into the cave.

A very prominent relationship exists between the $\delta^{18}O$, $\delta^{13}C$, and grayscale values (Figure 5.4), suggesting a common geological process or mechanism linking all three proxies together. Tropical climate variability is dominated by ENSO, such that during El Niño events in Costa Rica, enhanced orographic rainfall occurs on the Caribbean slope, while drier conditions occur on the Pacific slope (Waylen et al., 1996). Based on the amount effect (Dansgaard, 1964), drier conditions forced by El Niño produce higher $\delta^{18}O$ values. Less moisture leads to a decrease in biological respiration rates and produces higher $\delta^{13}C$ values. Due to drier

conditions, less water infiltrates through the soil zone, limestone bedrock, and into the cave system, producing slower drip rates into the cave and darker/denser calcite layers.

Since climate in the tropics is relatively stable throughout the year, the dominant control on climate variability in Costa Rica would be ENSO and/or the PDO. The paleoclimate record generated from stalagmite CT-7 demonstrates decadal rainfall variability throughout the interval of growth of CT-7, which can be interpreted as ENSO and PDO band variance.

Variations in the strength and frequency of ENSO and the PDO impact climate worldwide, due to the complex interaction between the ocean-atmosphere system in the tropical Pacific Ocean. Presently, ENSO operates on a 2-7 year frequency (Moy et al., 2002), but the paleoclimate record suggests that throughout the Holocene, ENSO has varied in both strength and frequency. By elucidating past variations in the ENSO cycle, the future will benefit from better ENSO predictions which can affect societies around the world. Determining ENSO and PDO variability throughout the Holocene will help resolve the history and dynamics of tropical Pacific climate variability.

APPENDIX I

STANDARD PROCEDURE - CARBONATE U-SERIES CHEMISTRY
(Modified from the University of Minnesota and applied at University of New Mexico)

1. Add a few drops of clean water to 30 ml teflon beaker (to avoid dispersing powder).
2. Add sample (~200 to 300 mg) then add enough water to cover sample (no more).
3. Add drops of 15N HNO_3 until fizzing stops.
4. Spike sample (~1 g of spike) - see spiking procedures.
5. Dry down.
6. Add a few drops of 15N HNO_3 until just wet. May need to reduce volume by heating.
7. Add a couple of drops of perchloric acid. Dry down.
8. Re-dissolve in 2N HCl (~2-4 ml), then add enough H_2O to ensure that the sample is entirely dissolved. (WARNING - do not use 6N HCl during this step.)
9. Transfer solution to centrifuge (CF) tubes. Use the 12 ml tubes.
10. Clean the 30 ml beaker with 6N HCl, then H_2O; ~1 ml at a time warming on a hot plate. Do this as you are centrifuging the sample after co-precipitation.
11. Add about 2 drops of Fe-solution.
12. Add water to make solution volume ~5 ml. (do not need to be exact)
13. Co-precipitate U & Th with ammonium hydroxide (NH_4OH). Add drops of NH_4OH until pH=7. You will see the Fe coagulate and precipitate.
14. Make sure that centrifuge canisters are balanced to within ~0.10 g.
15. After 4 minute CF at 2700 rpm, decant solution (do not loose precipitate!).
16. Wash with H_2O (add H_2O and stir with teflon rod), then add 1 drop of NH_4OH.
17. Repeat 4 minute centrifugation and decant solution.
18. Add ~4-5 drops 15N HNO_3 to dissolve precipitate and transfer back to 30 ml beaker.
19. Dry EASY.
20. Add another 3-4 drops 15N HNO_3 and dry down.
21. Sample ready to dissolve in 1 column volume 7N HNO_3 for loading into columns.

66

<u>Elution</u>
Sample size: 200 - 300 mg.
Columns: large = 500 µl, small = 150 µl.
Column and resin wash: 6 CV 6N HCl, 6 CV H_2O,
Clean Column reservoir: fill to brim with H_2O, let resin settle and empty
water
Column conditioning: 6 CV 7N HNO_3.

1st Stage of Column Work
large column = 500 µl
Load   1 CV 7N HNO_3
Clean   0.75 CV 7N HNO_3
Clean   0.75 CV 7N HNO_3
clean 30 ml beaker with ~1 ml of 6N HCl on hot plate, then with ~ 1 ml
water on hot plate. Rinse well with water.
Collect Th   4 CV 6N HCl
                  (1 CV, then 3 CV)
                  dry down
Collect U   1 CV H_2O
                  3 CV HBr (1N)
                  dry down
Add 3-4 drops 15N HNO_3, dry again easy.
Repeat.

2nd Stage of Column Work
small column = 150 µl
Load (Th)   1 CV 7N HNO_3
Clean   1 CV 7N HNO_3
Clean   1 CV 7N HNO_3 optional
Clean   1 CV 7N HNO_3 optional

Collect Th   3 CV 6N HCl   *Do not clean beaker!* (1 CV, then 2 CV)
                  dry down
Clean   10 CV H_2O
Condition   6 CV 7N HNO_3
Load (U)   1 CV 7N HNO_3
Clean   2 CV 7N HNO_3
Clean (optional) 2 CV 6N HCl

Collect U   1 CV H_2O Do not clean beaker!
              3 CV HBr (1N)
              dry down
Add 3-4 drops 15N HNO_3, dry again easy.

Yemane Asmerom, asmerom@unm.edu 505-277-4434
Victor Polyak, polyak@unm.edu 505-277-1640
Radiogenic Isotope Laboratory
Department of Earth and Planetary Sciences, University of New Mexico
200 Yale Blvd, Northrop Hall, Albuquerque, New Mexico 87131

APPENDIX II

STABLE ISOTOPE DATA

Dist from base (mm)	δ13C	δ18O	age	Dist. from base (mm)	δ13C	δ18O	age	Dist. from base (mm)	δ13C	δ18O	age
1	-8.21	-8.42	7895	59	-10.50	-8.85	7675	116	-10.39	-8.72	7458
2	-9.06	-8.67	7891	60	-9.75	-8.01	7671	117	-10.62	-8.69	7455
3	-10.10	-8.47	7887	61	-9.63	-7.89	7667	118	-11.63	-9.14	7451
4	-11.24	-8.87	7883	62	-10.20	-8.17	7663	119	-10.24	-8.76	7447
5	-10.26	-8.72	7879	63	-10.35	-8.02	7659	120	-10.08	-8.68	7443
7	-11.09	-8.93	7872	64	-10.04	-8.07	7656	121	-10.08	-7.98	7439
8	-10.67	-8.35	7868	65	-10.62	-8.49	7652	122	-9.98	-8.39	7436
9	-10.59	-8.09	7864	66	-10.19	-8.09	7648	123	-9.29	-8.24	7432
10	-10.61	-8.57	7860	67	-11.03	-8.84	7644	124	-9.17	-8.79	7428
11	-11.03	-9.32	7857	68	-9.99	-7.87	7640	125	-9.53	-8.82	7424
12	-10.89	-8.80	7853	69	-10.81	-8.09	7637	126	-10.21	-8.57	7420
13	-10.71	-8.59	7849	70	-11.25	-8.70	7633	127	-10.09	-8.21	7417
14	-10.24	-8.35	7845	71	-10.56	-8.53	7629	128	-10.12	-8.30	7413
15	-11.35	-8.69	7841	72	-11.12	-8.59	7625	129	-9.75	-8.93	7409
16	-10.09	-8.11	7838	73	-10.75	-8.64	7621	130	-9.57	-8.67	7405
17	-10.62	-9.15	7834	74	-10.30	-8.31	7618	131	-9.85	-8.52	7402
18	-11.51	-8.62	7830	75	-10.96	-8.52	7614	132	-10.37	-8.60	7398
19	-11.19	-8.90	7826	76	-9.36	-7.31	7610	133	-10.71	-8.59	7394
20	-10.71	-8.52	7822	77	-10.34	-8.61	7606	134	-10.58	-8.51	7390
21	-11.37	-8.76	7819	78	-9.36	-8.44	7603	135	-9.57	-8.53	7386
22	-10.63	-8.31	7815	79	-10.19	-7.72	7599	136	-9.25	-8.21	7383
23	-9.89	-8.20	7811	80	-9.68	-8.49	7595	137	-9.01	-6.37	7379
24	-10.93	-8.66	7807	81	-9.52	-8.21	7591	138	-10.02	-8.58	7375
25	-10.30	-8.44	7804	82	-9.84	-8.17	7587	139	-10.19	-8.71	7371
26	-10.85	-8.01	7800	83	-8.93	-7.48	7584	140	-10.32	-8.66	7367
27	-11.60	-8.95	7796	84	-8.30	-8.02	7580	141	-9.93	-8.55	7364
28	-11.94	-8.82	7792	85	-9.60	-8.38	7576	142	-10.62	-8.89	7360
29	-11.17	-8.09	7788	86	-9.41	-8.40	7572	143	-10.29	-8.73	7356
30	-11.12	-8.67	7785	87	-9.47	-8.17	7568	144	-10.00	-8.96	7352
31	-11.11	-8.34	7781	88	-10.05	-8.45	7565	145	-9.53	-8.29	7348
32	-10.39	-8.38	7777	89	-10.48	-8.64	7561	146	-11.12	-9.12	7345
33	-10.62	-8.41	7773	90	-10.04	-8.47	7557	147	-11.07	-8.95	7341
34	-11.04	-8.44	7769	91	-10.81	-8.44	7553	148	-10.60	-8.53	7337
35	-11.37	-8.46	7766	92	-10.48	-8.58	7549	149	-8.68	-7.82	7333
36	-9.83	-7.78	7762	93	-10.70	-8.64	7546	150	-9.20	-8.33	7329
37	-10.89	-8.27	7758	94	-10.66	-8.75	7542	151	-7.91	-8.10	7326
38	-11.27	-8.60	7754	95	-8.55	-7.31	7538	152	-9.96	-8.71	7322
39	-11.00	-8.72	7750	96	-10.42	-8.32	7534	153	-9.37	-8.09	7318
40	-9.53	-8.30	7747	97	-10.52	-10.08	7530	154	-9.28	-7.76	7314
41	-10.15	-8.10	7743	98	-10.19	-8.31	7527	155	-9.89	-8.41	7311
42	-10.44	-8.30	7739	99	-9.51	-7.80	7523	156	-9.36	-8.64	7307
43	-9.61	-8.30	7735	100	-10.67	-8.28	7519	157	-9.09	-8.14	7303
44	-10.19	-8.45	7731	101	-10.42	-8.08	7515	158	-8.59	-6.91	7299
45	-10.97	-8.70	7728	102	-10.20	-8.22	7512	159	-9.09	-7.92	7295
46	-10.77	-8.31	7724	103	-10.64	-8.60	7508	160	-9.17	-8.28	7292
47	-10.66	-8.05	7720	104	-9.88	-8.61	7504	161	-9.87	-8.00	7288
48	-11.06	-8.42	7716	105	-9.42	-8.33	7500	162	-9.51	-7.93	7284
49	-10.68	-8.38	7712	106	-9.59	-8.52	7496	163	-9.73	-8.27	7280
50	-10.27	-8.24	7709	107	-9.54	-8.12	7493	164	-9.07	-8.13	7276
51	-11.19	-8.97	7705	108	-9.80	-8.21	7489	165	-8.84	-8.12	7273
52	-11.54	-8.90	7701	109	-9.52	-8.12	7485	166	-9.23	-7.99	7269
53	-10.79	-8.37	7697	110	-9.75	-8.41	7481	167	-10.06	-9.13	7265
54	-11.73	-9.02	7694	111	-10.27	-8.95	7477	168	-10.35	-8.52	7261
55	-10.31	-8.24	7690	112	-10.45	-8.70	7474	169	-9.51	-8.44	7257
56	-9.27	-8.28	7686	113	-10.37	-8.72	7470	170	-9.42	-8.78	7254
57	-9.09	-8.21	7682	114	-10.39	-8.73	7466	171	-9.56	-8.58	7250
58	-9.02	-8.47	7678	115	-10.05	-8.57	7462	172	-10.49	-8.47	7246

Note: $\delta^{18}O$ and $\delta^{13}C$ values represented in ‰ notation relative to VPDB

69

Dist from base (mm)	δ13C	δ18O	age	Dist. from base (mm)	δ13C	δ18O	age	Dist. from base (mm)	δ13C	δ18O	age
173	-9.60	-7.95	7242	231	-8.97	-7.54	7022	288	-9.71	-7.70	6806
174	-9.09	-8.01	7238	232	-8.45	-7.37	7018	289	-9.91	-8.01	6802
175	-8.18	-8.02	7235	233	-9.04	-7.74	7015	290	-10.15	-7.87	6799
176	-7.92	-7.83	7231	234	-7.81	-7.68	7011	291	-9.41	-7.67	6795
177	-8.57	-7.67	7227	235	-9.06	-8.33	7007	292	-10.35	-8.20	6791
178	-8.80	-8.50	7223	236	-7.24	-7.34	7003	293	-11.03	-8.59	6787
179	-8.42	-7.96	7219	237	-6.85	-7.61	7000	294	-10.88	-8.52	6783
180	-10.13	-8.42	7216	238	-8.73	-7.83	6996	295	-10.22	-7.96	6780
181	-9.34	-8.43	7212	239	-9.09	-8.13	6992	296	-9.94	-7.43	6776
182	-7.88	-7.66	7208	240	-8.34	-7.63	6988	297	-9.60	-8.39	6772
183	-7.64	-7.72	7204	241	-8.59	-7.61	6984	298	-9.16	-7.79	6768
184	-8.63	-8.22	7201	242	-9.03	-8.24	6981	299	-9.04	-7.69	6764
185	-9.37	-8.43	7197	243	-8.35	-8.04	6977	300	-10.14	-8.03	6761
186	-8.05	-7.99	7193	244	-9.22	-8.28	6973	301	-10.30	-8.40	6757
187	-9.35	-8.35	7189	245	-9.64	-8.07	6969	302	-10.73	-8.57	6753
188	-8.86	-7.86	7185	246	-10.11	-9.15	6965	303	-10.45	-8.37	6749
189	-8.56	-8.03	7182	247	-10.12	-7.90	6962	304	-9.35	-8.40	6745
190	-8.70	-8.08	7178	248	-9.77	-8.10	6958	305	-7.95	-7.75	6742
191	-7.50	-7.38	7174	249	-9.32	-8.10	6954	306	-8.75	-8.60	6738
192	-8.43	-7.44	7170	250	-10.49	-8.58	6950	307	-9.10	-8.28	6734
193	-9.11	-7.63	7166	251	-10.17	-8.38	6946	308	-9.07	-8.65	6730
195	-8.87	-7.63	7159	252	-9.55	-8.52	6943	309	-9.31	-8.68	6726
196	-8.99	-7.57	7155	253	-10.62	-8.43	6939	310	-8.61	-8.30	6723
197	-9.31	-8.33	7151	254	-11.61	-8.93	6935	311	-9.32	-7.95	6719
198	-9.45	-9.03	7147	255	-10.85	-8.69	6931	312	-9.54	-8.27	6715
199	-9.17	-8.31	7144	256	-10.32	-8.53	6927	313	-9.47	-8.11	6711
200	-10.17	-9.02	7140	257	-10.99	-8.36	6924	314	-9.98	-8.70	6708
201	-11.04	-8.84	7136	258	-10.77	-8.93	6920	315	-9.40	-8.59	6704
202	-9.50	-8.27	7132	259	-10.04	-8.27	6916	316	-8.65	-8.94	6700
203	-8.97	-7.94	7128	260	-10.33	-8.19	6912	317	-8.18	-7.76	6696
204	-9.87	-8.90	7125	261	-11.02	-8.92	6909	318	-7.89	-8.25	6692
205	-10.21	-9.20	7121	262	-9.43	-8.33	6905	319	-8.35	-8.87	6689
206	-10.63	-10.00	7117	263	-9.74	-8.24	6901	320	-7.27	-7.39	6685
207	-9.13	-8.39	7113	264	-10.34	-8.50	6897	321	-8.17	-8.19	6681
208	-9.58	-8.61	7110	265	-9.62	-8.33	6893	322	-9.08	-8.34	6677
209	-9.65	-8.72	7106	266	-9.47	-8.11	6890	323	-11.00	-8.12	6673
210	-10.07	-9.30	7102	267	-9.96	-7.94	6886	324	-10.29	-8.52	6670
211	-9.85	-8.66	7098	268	-10.01	-7.97	6882	325	-11.46	-9.09	6666
212	-9.42	-8.69	7094	269	-9.62	-7.89	6878	326	-11.51	-8.61	6662
213	-9.21	-8.32	7091	270	-10.50	-8.85	6874	327	-11.16	-8.57	6658
214	-8.69	-9.00	7087	271	-10.03	-7.87	6871	328	-10.72	-8.85	6654
215	-8.71	-8.70	7083	272	-10.64	-7.98	6867	329	-9.83	-8.93	6651
216	-9.27	-8.22	7079	273	-9.94	-8.23	6863	330	-9.28	-8.65	6647
217	-8.58	-7.57	7075	274	-10.02	-8.71	6859	331	-8.46	-8.14	6643
218	-9.10	-7.52	7072	275	-10.83	-8.09	6855	332	-8.67	-8.14	6639
219	-8.68	-7.51	7068	276	-9.60	-7.77	6852	333	-10.10	-9.02	6635
220	-8.73	-7.85	7064	277	-10.06	-7.36	6848	334	-10.54	-9.30	6632
221	-9.51	-8.06	7060	278	-10.31	-8.59	6844	335	-10.75	-8.31	6628
222	-9.03	-8.29	7056	279	-10.07	-7.94	6840	336	-11.45	-9.07	6624
223	-8.33	-7.94	7053	280	-10.55	-8.68	6836	337	-9.97	-8.40	6620
224	-8.12	-7.28	7049	281	-10.54	-10.17	6833	338	-10.25	-8.43	6617
225	-7.61	-6.69	7045	282	-9.20	-7.64	6829	339	-10.18	-8.27	6613
226	-8.68	-7.65	7041	283	-9.92	-7.67	6825	340	-10.47	-8.33	6609
227	-8.39	-7.54	7037	284	-9.53	-7.96	6821	341	-11.77	-9.75	6605
228	-8.30	-7.50	7034	285	-9.51	-7.49	6818	342	-11.11	-8.94	6601
229	-8.00	-7.49	7030	286	-9.67	-7.58	6814	343	-11.20	-8.82	6598
230	-9.05	-7.60	7026	287	-10.10	-7.90	6810	344	-11.43	-9.11	6594

70

Dist from base (mm)	δ13C	δ18O	age
345	-11.16	-8.76	6590
346	-11.14	-8.21	6586
347	-11.13	-8.49	6582
348	-10.96	-8.28	6579
349	-9.78	-8.09	6575
350	-10.07	-8.12	6571
351	-7.93	-8.00	6567
352	-9.26	-8.48	6563
353	-9.71	-8.26	6560
354	-8.51	-8.05	6556
355	-9.10	-8.09	6552
356	-9.59	-8.06	6548
357	-10.26	-8.44	6544
358	-9.72	-8.39	6541
359	-9.31	-8.20	6537
360	-8.46	-7.86	6533
361	-8.89	-7.98	6529
362	-8.74	-8.19	6525
363	-9.22	-8.55	6522
364	-9.10	-8.38	6518
365	-10.99	-8.57	6514
366	-10.61	-8.30	6510
367	-10.13	-8.06	6507
368	-9.81	-8.09	6503
369	-9.89	-8.11	6499
370	-9.46	-7.77	6495
371	-8.22	-7.29	6491
372	-6.84	-7.16	6488

REFERENCES

Arrigo, R.D., Villalba, R., and Wiles, G., 2001, Tree-ring estimates of Pacific climate variability: Climate dynamics, v.18, p. 219-224.

Baker, A., Ito, E., Smart, P.L. and McEwan, R.F., 1997, Elevated and variable values of (super 13) C in speleothems in a British cave system: Chemical Geology, v. 136, p. 263-270.

Baker, A., Proctor, C.J., and Barnes, W.L., 1999, Variations in stalagmite luminescence laminae structure at Poole's Cavern, England, AD 1910-1996: calibration of palaeoprecipitation proxy: The Holocene, v. 9, p. 683-688.

Baskaran, M., and Krishnamurthy, R.V., 1993, Speleothems are proxy for carbon isotope composition of atmospheric CO_2: Geophysical Research Letters, v. 20, p. 2905-2908.

Biondi, F., Gershunov, A., and Cayan, D.R., 2001, North Pacific decadal climate variability since 1661: Journal of Climate, v. 14, p. 5-10.

Blanchon, P. and Shaw, J., 1995, Reef drowning during the last deglaciation: evidence for catastrophic sea-level rise and ice-sheet Collapse: Geology, v. 23, p. 4-8.

Bond, G., Kromer, B., Beer, J., Muscheler, R., Evans, M.N., Showers, W., Hoffman, S., Lotti-Bond, R., Hajdas, I., and Bonani, G., 2001, Persistent solar influence on North Atlantic climate during the Holocene: Science, v. 294, p. 2130-2136.

Burns, S.J., Fleitmann, D. Mudelsee, M., Neff, U., Matter, A., and Mangini, A., 2002, A 780- yr annually resolved record of Indian Ocean monsoon and precipitation from a speleothem from Southern Oman: Journal of Geophysical Research D. Atmospheres, v. 107, p. 9.

Cane, M.A., 2005, The evolution of El Niño, past and future: Earth and Planetary Science Letters, v. 164, p. 1-10.

Castillo-Munoz, R., 1983, Geology *in*, Janzen, D.H., editor, Costa Rican Natural History: Chicago, University of Chicago Press, 816 p.

Charles, C.D., Cobb, K., Moore, M.D., and Fairbanks, R.G., 2003, Monsoon-tropical ocean interaction in a network of coral records spanning the 20th century: Marine Geology, v. 201, p. 207-222.

Clark, P.U., Alley, R.B., Pollard, D., 1999, Northern Hemisphere ice-sheet influences on global climate change, Science, v. 286, p. 1104-11.

Clement, A.C., Seager, R., and Cane, M.A., 1999, Orbital controls on the El Niño/Southern Oscillation and the tropical climate: Paleoceanography, v. 14, p.441-456.

Clement, A.C., Seager, R., and Cane, M.A., 2000, Suppression of El Niño during the mid-Holocene by changes in the earth's orbit: Paleoceanography, v. 15, p. 731-737.

Cobb, K.M., Charles, C.D., Cheng, H., and Edwards, R.L., 2003, El Nino/Southern Oscillation and tropical Pacific climate during the last millennium: Nature, v. 424, p. 271-276.

Coen, E., 1983, Climate *in*, Janzen, D.H., editor, Costa Rican Natural History: Chicago, University of Chicago Press, 816 p.

Cole, Julia E., R. G. Fairbanks, and G. T. Shen.,1993, Recent variability in the Southern Oscillation: isotopic results from a Tarawa Atoll Coral: Science, v. 260, p. 1790 - 1793.

Cole, J., 2001, A slow dance for El Niño: Science, v. 291, p. 1496-1497.

Cook, E.R., Woodhouse, C.A., Eakin, C.M., Meko, D.M., and Stahle, D.W., 2004, Long-Term aridity changes in the Western United States: Science, v. 306, p. 1015-1018.

Curtis, J.H., Brenner, M., Hodell, D.A., Balser, R.A., Islebe, G.A., and Hooghiemstra, H., 1998, A multi-proxy study of Holocene environmental change in the Maya Lowlands of Peten, Guatemala: Journal of Paleolimnology, v. 19, p. 139-159.

Curtis, J.H., Brenner, M., and Hodell, D.A, 1999, Climate change in the Lake Valencia Basin, Venezuela, ~12600 yr BP to present: The Holocene, v. 9, p. 609-619.

73

Dansgaard, W., 1964, Stable isotopes of precipitation: Tellus, v. 16, p. 436-468.

Dansgaard, W., Johnsen, S.J., Clausen, H.B., Dahl-Jensen, D., Gundestrup, N.S., Hammer, C.U., Hvidberg, C.S., Steffensen, J.P., Sveinbjörnsdóttir, A.E., Jouzel, J., and Bond, G.C.,1993, Evidence for general instability of past climate from a 250 kyr ice-core record: Nature, v. 264, p. 218-220.

Darling, W.G., 2004, Hydrological factors in the interpretation of stable Isotope proxy data present and past: a European perspective: Quaternary Science Reviews, v. 23, p. 743-770.

Dorale, J.A., González, L.A., Reagan, M.K., Pickett, D.A., Murrell, M.T., and Baker, R.G., 1992, A high-resolution record of Holocene climate change in speleothem calcite from Cold Water Cave, northeast Iowa: Science, v. 258, p. 1626-1630

Dorale, J.A., Edwards, R.L., Ito, E., and Gonzalez, L.A., 1998, Climate and vegetation history of the mid-continent from 75-25ka: A speleothem record from Crevice cave, Missouri, USA: Science, v. 282, p. 1871-1874.

Dorale, J.A., Edwards, R.L., Alexander, E.C., Shen, C.C., Richards, D.A., and Cheng, H., 2004, Uranium-series dating of speleothems: current techniques, limits and applications, In: Sasowsky,I.D., Mylorie, J. (eds), Studies of Cave Sediments. Physical and Chemical Records of Palaeoclimate: Kluwer Academic, New York, p. 177-197.

Duque-Caro, H., 1990, Neogene stratigraphy, palaeoceanography and Paleobiogeography in northwest South America and the evolution Of the Panama Seaway: Palaeogeography, Palaeoclimataology, Palaecology, v. 77, p. 203-234.

Enfield D.B., Cid L.S., 1991, Low-frequency changes in El Niño- Southern Oscillation: Journal of Climate, v. 4, p. 1137-1146

Enfield, D.B., and Alfaro, E.J., 1999, The dependence of Caribbean rainfall on the interaction of the tropical Atlantic and Pacific oceans: Journal of Climate, v. 12, p. 2093-2103.

Evans, M.N., Cane, M.A., Schrag, D.P., Kaplan, A., Linsley, B.K., Villalba, R., and Wellington, G.M., 2001, Support for tropically-driven decadal variability based on paleoproxy evidence: Geophysical Research Letters, v. 28, p. 3689-3692.

Fairchild, I.J., Smith, C.L., Baker, A., Fuller, L., Spotl, C., Mattey, D., McDermott, F., and E.I.M.F., 2006, Modification and preservation of environmental signals in speleothems: Earth Science Reviews (in press)

Fairchild, I.J., Frisia, S., Borsato, A. and Tooth, A.F., 2006, Speleothems. *In* Geochemical Sediments and Landscapes (ed. Nash, D.J. and McLaren, S.J.), Blackwells, Oxford (in press)

Fantidis, J., and Ehhalt, D.H., 1970, Variations of the carbon and oxygen isotopic composition in stalagmites and stalactites: Evidence of non-equilibrium isotopic fractionation: Earth and Planetary Science Letters, v. 10, p. 136-144.

Fleitmann, D., Burns, B.J., Neff, U., Mudelsee, M., Mangini, A., and Matter, A., 2004, Palaeoclimatic interpretation of high- resolution oxygen isotope profiles derived from annually laminated speleothems from Southern Oman: Quaternary Science Reviews, v. 23, p. 935-945.

Fleitmann, D., Burns, S.J., Mudelsee, M., Neff, U., Kramers, J., Mangini, A., Matter, A.,2003, Holocene forcing of the Indian Monsoon recorded in a stalagmite from southern Oman: Science, v. 300, p. 1737-1739.

Frankie, G.W., Baker, H.G., and Opler, P.A., 1974, Comparative phonological studies of trees in tropical wet and dry forests in the lowlands of Costa Rica: Journal of Ecology, v. 62, p. 881-919.

Frappier, A., Sahagian, D., Gonzalez, L.A., and Carpenter, S.J., 2002, El Niño events recorded by stalagmite carbon isotopes: Science, v. 298, p. 565.

Friedman, I. and O'Neil, J.R., 1977. Compilation of stable isotope fractionation factors of geochemical interest. In: M.Fleischer (Ed), Data of Geochemistry: U.S. Geological Survey Professional Paper 440-KK, 6th Ed.

Fritts, H. C., Vaganov, E.A., Sviderskaya, I.V., and Shashkin, A.V., 1991, Climatic variation and tree-ring structure in conifers: Empirical and mechanistic models of tree-ring width, number of cells, cell size, cell-wall thickness and wood density: Climate Research, v. 1, p. 97-116.

Gagan, K.M., Ayliffe, L.K., Beck, J.W., Cole, J.E., Druffel, E.R.M, Dunbar, R.B., and Schrag, D.P., 2000, New views of tropical paleoclimates from corals: Quaternary Science Reviews, v. 19, p. 45-64.

Gascoyne, M., 1977, Trace element geochemistry of speleothems. Proceedings of the 7th International Speleology Congress, Sheffield, England, p. 205-207.

Gascoyne, M., 1992, Paleoclimate determination from cave calcite deposits: Quaternary Science Reviews, v. 11, p. 609-632.

Genty, D., and Quinif, Y., 1996, Annually laminated sequences in the internal structure of some Belgian stalagmites; importance for paleoclimatology: Journal of Sedimentary Research, v. 66, p. 275-288.

Genty, D., Baker, A., Massault, M., Proctor, C., Gilmour, M., Pons-Branchu, E., and Hamelin, B., 2001, Dead carbon in stalagmites: carbonate bedrock paleodissolution vs. ageing of soil organic matter. Implications for ^{13}C variations in speleothems: Geochemica et Cosmochimica Acta, v.65, p. 3443-3457.

Giannini, A., Kushnir, Y., and Cane, M.A., 2000, Interannual variability of Caribbean rainfall, ENSO, and the Atlantic Ocean: Journal of Climate, v. 13, p. 297-311.

Gilson, J.R., and MacCarthney, E., 1954, Luminescence in speleothems from Devon, UK: the presence of organic activators: Ashford Speleological Society, v. 6, p. 8-11.

Gray, S.T., Betancourt, J.L., Fastie, C.L., and Jackson, S.T., 2003, Patterns and sources of multidecadal oscillations in drought sensitive tree ring records from the central and southern Rocky Mountains: Geophysical Research Letters, v. 30. p. 1-6.

Gupta, A.K., Anderson, D.M., and Overpeck, J.T., 2003, Abrupt changes in the Asian southwest monsoon during the Holocene and their links to the North Atlantic Ocean: Nature, v. 421. p. 354-357.

Hartshorn, G.S., 1983, Plants *in*, Janzen, D.H., editor, Costa Rican Natural History: Chicago, University of Chicago Press, 816 p.

Hastenrath, S., 1978, On modes of tropical circulation and climate anomalies: Journal of the Atmospheric Sciences, v. 2, p. 2222-2231.

Harmon, R.S., and Curl, R.E., 1978, Preliminary results on growth rate and paleoclimate studies of a stalagmite from Ogle Cave, New Mexico: National Speleological Society Bulletin., v. 40, p. 25-26 (disc. & reply, v. 40, p. 123-124).

Harmon, R.S., Schwarcz, H.P., and Ford, D.C., 1978, Stable isotope geochemistry of speleothems and cave waters from the Flint Ridge-Mammoth Cave system, Kentucky: Implications for terrestrial change during the period 230,000 to 100,000 years B.P.: Journal of Geology, v. 86, p. 373-384.

Harmon, R.S., Thompson, P., Schwarcz, H.P. et al., 1978, Late Pleistocene paleoclimates of North America as inferred from stable isotope studies of speleothems: Quaternary Research, v. 9, p. 54-70.

Haug, G.H., Hughen, K.A., Sigman, D.M., Peterson, L.C., and Roehl, U., 2001, Southward migration of the Intertropical Convergence Zone through the Holocene: Science, v. 293, p. 1304-1308.

Hempell, J.C., 1989, Report of the 1982 expedition to Barra Honda National Park, In: Schomar, B., Randall, B., and Werner, E. (eds), Bulletin 1, National Speleological Society Costa Rica Project

Hendy, C.H., 1971, The isotopic geochemistry of speleothems-1. The calculation of the effects of different modes of formation on the isotopic composition of speleothems and their applicability as palaeoclimatic indicators: Geochemica et Cosmochemica Acta, v. 35, p. 801-824.

Hodell, D.A., Curtis, J.H., Jones, G.A., Higuera-Gundy, A., Brenner, M, Binford, M.W., and Dorsey, K.T., 1991, Reconstruction of Caribbean climate change over the past 10500 years: Nature, v. 352, p. 790-793.

Hodell, D.A., Curtis, J.H., and Brenner, M., 1995, Possible role of climate in the collapse of Classic Maya civilization: Nature, v. 375, p. 391-394.

Hughen, K.A., Schrag, D.P., and Jacobsen, S.B., 1999, El Niño during the last interglacial period recorded by a fossil coral from Indonesia: Geophysical Research Letters, v. 26, p. 3129 - 3132.

James, J.M., 1997, Minor, trace and ultra-trace constituents of speleothems: In: Hill, C.A. and Forti, P. (eds) Cave minerals of the world: National Speleological Society, 236-237

Jones, I.C., Banner, J.L., and Humphrey, J.D., 2000, Estimating recharge in a tropical karst aquifer: Water Resources Research, v. 36, p. 1289-1299.

Kessler, W.S., Frequently Asked Questions about El Niño, *in* Babkina, A.M., editor, 2003, El Niño: Overview and Bibliography, Nova Science Publishers, Inc, New York, 196 p.

Kim, S., and O'Neil, J.R., 1997, Equilibrium and nonequilibrium oxygen isotope effects in synthetic carbonates: Geochimica et Cosmochimica, v. 61, p. 3461-3475.

Koutavas, A., Lynch-Stieglitz, J., Marchitto, T.M., and Sachs, J.P., 2002, El Niño-like pattern in ice age tropical Pacific sea surface temperature: Science, v. 297, p. 226-230.

Lachniet, M.S., and Patterson, W.P., 2002. Stable isotope values of Costa Rican surface waters: Journal of Hydrology, v. 260, p. 135-150.

Lachniet, M.S., Asmerom, Y., Burns, S.J., Patterson, W.P., Polyak, V.J., and Seltzer, G.O., 2004, Tropical response to the 8200 yr B.P. cold event? Speleothem isotopes indicate a weakened early Holocene monsoon in Costa Rica: Geology, v. 32, p. 957-960.

Lachniet, M.S., Burns, S.J., Piperno, D.R., Asmerom, Y., Polyack, V.J., Moy, C.M., and Christenson, K., 2004, A 1500-year El Niño /Southern Oscillation and rainfall history for the Isthmus of Panama from speleothem calcite: Journal of Geophysical Research, v. 109, p. 1-8.

Lachniet, M.S. and Patterson, W.P., 2006. Use of correlation and multiple stepwise regression to evaluate the climatic controls on the stable isotope values of Panamanian surface waters: Journal of Hydrology, (in press)

Lauritzen, S.E., and Lundberg, J., 1999, Speleothems and climate: a special issue of the Holocene: The Holocene, v. 9, p. 643-647.

Linsley, B.K., Dunbar, R.B., Wellington, G.M., Mucciarone, D.A., 1994, A coral-based reconstruction of Intertropical Convergence Zone variability over Central America since 1707: Journal of Geophysical Research, v. 99, p. 9977-9994.

Lluch-Cota, D.B., Wooster, W.S., and Hare, S.R., 2001, Sea surface temperature variability in coastal areas of the Northeastern Pacific related to the El Nino-Southern Oscillation and Pacific Decadal Oscillation: Geophysical Research Letters, v. 28. p. 2029-2032.

Ludwig, K.R., 2003, User's manual for Isoplot 3.00, a geochronological toolkit for Microsoft Excel: Berkeley Geochronology Center Special Publication, No. 4, 74pp.

Mantua, N.J., Hare, S.R., Zhang, Y., Wallace, J.M., and Francis, R.C., 1997, A Pacific Interdecadal oscillation with impacts on salmon Production: Bulletin of American Meteorology Society, v. 78, p. 1069-1079.

Mantua, N.J., and Hare, S.R., 2002, The Pacific decadal oscillation: Journal of Oceanography, v. 58, p.35-44.

McDermott, F., 2004, Palaeo-climate reconstruction from stable isotope variations in speleothems: a review: Quaternary Science Reviews, v. 23, p. 901-918.

Mickler, P.J., Banner, J.L., Stern, L., Asmerom, Y., Edwards, L.R. and Ito, Emi, 2004, Stable isotope variations in modern tropical speleothems: Evaluating equilibrium vs. kinetic isotope effects: Geochemica at Cosmochimica Acta, v. 68, p. 4381-4393.

Minobe, S., 1997, A 50-70 year climatic oscillation over the North Pacific and North America: Geophysical Research Letters, v. 24, p. 683-686.

Minobe, S., 1999, Resonance in bidecadal and pentadecadal climate oscillations over the North Pacific: Role in climatic regime shifts: Geophysical Research Letters, v. 26, p. 855-858.

Mora, S., 1992, Controls on karst in Costa Rica: International Contributions to Hydro-geology, v. 13, p. 467-474.

Moura, A.D., and Shukla, J., 1981, On the dynamics of droughts in Northwest Brazil: Observations, theory and numerical experiments with a general circulation model: Journal of Atmospheric Science, v. 38, p. 2653-2675.

Moy, C. M., Seltzer, G.O., Rodbell, D.T., and Anderson, D.M., 2002, Variability of El Niño/Southern Oscillation activity at millennial timescales during the Holocene epoch: Nature, v. 420, p. 162-165.

Neff, U., Burns, S.J., Mangini, A., Mudelsee, M., Fleitmann, D., and Matter, A., 2001, Strong coherence between solar variability and monsoon in Oman between 9 and 6 kyr ago: Nature, v. 411, p. 290-293.

Newman, M., Compo, G.P., and Alexander, M.A.,2003, ENSO-forced variability of the Pacific Decadal Oscillation, Journal of Climate, v. 16, p. 3853-3857.

NOAA, 2006, National Ocean and Atmospheric Administrative. El Niño Theme Page. Accessible at: http://www.pmel.noaa.gov/tao/elnino/nino-home.html

Otto-Bliesner, B.L., 1999, El Niño/La Nina and Sahel precipitation During the middle Holocene: Geophysical Reseach Letters, v. 26, p. 87-90.

Polyak, V.J., and Asmerom, Y., 2001, Late Holocene climate and cultural changes in the southwestern United States: Science, v. 294, p. 148-151.

Richards, D.A., and Dorale, J.A., 2003, Uranium-series and environmental applications of speleothems: Review of Mineralogy and Geochemistry, v. 52, p. 407-460.

Rodbell, D.T., Seltzer, G.O., Anderson, D.M., Abbott, M.B., Enfield, D.B., and Newman, J.H., 1999, A ~15,000- yr record of El Niño-driven alluviation in southwestern Ecuador: Science, v. 283, p. 516-520.

Ropelewski, C.F., and Halpert, M.S., 1987, Global and regional scale precipitation patterns associated with the El Niño /Southern Oscillation: Monthly Weather Review, v. 115, p. 1606-1626.

Rozanski, K., Araguas, L.A., and Gonfiantini, 1993, Isotopic patterns in modern global precipitation *in* Swart, P.K., Lohmann, K.C., McKenzie, J., and Savin, S., eds., Climate Change in Continental Isotopic Records: American Geophysical Union, v. 78, p. 1-36.

Sandweiss, D.H., Maasch, K.A., Burger, R.L, Richardson III, J.B., Rollins, H.B., and Clement, A.C., 2001, Variation in Holocene El Niño frequencies: Climate records and cultural consequences in ancient Peru: Geology, v. 29, p. 603-606.

Schulz, M., and Mudelsee, M., 2002, REDFIT: Estimating red-noise spectra directly from unevenly spaced paleoclimatic time series: Computers and Geosciences, v. 28, p. 421–426.

Shopov, Y.Y., Ford, D.C., and Schwarcz, H.P., 1994, Luminescent microbanding in speleothems: high resolution chronology and palaeoclimate: Geology, v. 22, p. 407-410.

Stuiver, M., and Braziunas, T.F., 1993, Sun, ocean, climate and atmospheric $^{14}CO_2$: An evaluation of causal and spectral relationships: Holocene, v. 3, p. 289-305.

Stuiver, M., Reimer, P.J., Bard, E., Beck, J.W., Burr, G.S., Hughen, K.A., Kromer, B., McCormac, F.G., Plicht, J.V.D., and Spurk, M., 1998, INTCAL98 Radiocarbon Age Calibration, 24,000-0 cal BP: Radiocarbon, v. 40, p. 1041-1083.

Torrence, C. and Compo, G.P., 1998, A Practical Guide to Wavelet Analysis: Bulletin of the American Meteorological Society, v. 79, p. 61-78.

Tudhope, A.W., Chilcott, C.P., McCulloch, M.T., Cook, E.R., Chappell, J., Ellam, R.M., Lea, D.W., Lough, J.M., and Shimmield, G.B., 2001, Variability in the El Niño-Southern Oscillation through a Glacial-Interglacial cycle: Science, v. 291, p. 1511-1517.

USGS GTOPO30 data set, 1996, US Geological Survey

Vaks, A., Bar-Matthews, M., Ayalon, A., Schilman, B., Gilmour, M., Hawkesworth, C.J., Frumkin, A., Kaufman, A., and Matthews, A., 2003, Paleoclimate reconstruction based on the timing of speleothem growth and oxygen and carbon isotope composition in a cave located in the rain shadow of Israel: Quaternary Research, v. 59, p. 182-193.

Van Beynen, P., Bourbonniere,R., Ford, D., and Schwarcz, H., 2001, Causes of colour and fluorescence in speleothems: Chemical Geology, v. 175, p. 319-341.

Vuille, M., Bradley, R.S., Werner, M., Healy, R., and Keimeg, F., 2003, Modeling ^{18}O in precipitation over the tropical Americas: 1. Interannual variability and climatic controls: Journal of Geophysical Research, v. 108, p. 1-24.

Waylen, P.R., Quesada, M.E., and Caviedes, C.N., 1996, Temporal and spatial variability of annual precipitation in Costa Rica and the Southern Oscillation: International Journal of Climatology, v. 16, p. 173-193.

Waylen, P.R., and Harrison, M., 2005, The coincidence of daily rainfall events in Liberia, Costa Rica and tropical cyclones in the Caribbean basin: International Journal of Climatology, v. 25, p. 1665-1674

White, W.B., Paleoclimate records from speleothems in limestone caves *in* Sasowsky, I.D., and Mylroie, J., eds, Studies of Cave Sediments: New York, Kluwer Academic/Plenum Publishers, p. 135-176.

Yapp, C.J., 1982, A model for the relationships between precipitation, D/H ratios, and precipitation intensity: Journal of Geophysical Research,

VITA

Graduate College
University of Nevada, Las Vegas

April Dianne Azouz

Home Address:
    5984 Turhan Circle
    Las Vegas, NV 89146

Degrees:
    Bachelor of Science, Earth Science, 2004
    Boston University

Thesis Title:
    Evidence of an active ENSO and PDO during the mid-Holocene from a
    Costa Rican speleothem

Thesis Examination Committee:
    Chairperson, Dr. Matthew Lachniet, Ph.D.
    Committee Member, Dr. Ganqing Jiang, Ph.D.
    Committee Member, Dr. Michael Nicholl, Ph. D.
    Graduate Faculty Representative, Dr. Barbara Luke, Ph.D.

83